Magyarhoni Földtani Társulat
Földtani Közlöny
Hungarian Geological Society

155/3, 213–233., Budapest, 2025

DOI: 10.23928/foldt.kozl.2025.155.3.213

Fracture-controlled paleofluid migration in the Óbánya Valley (Eastern Mecsek)

LADÁNYI, Lili[1,2], HRABOVSZKI, Ervin[1,3], SCHUBERT, Félix[1]

[1]Department of Geology, University of Szeged
[2]HUN-REN Biological Research Center, Szeged
[3]Department of Mineralogy and Geology, University of Debrecen

E-mail: ladanyi.lili.02@szte.hu

Törésrendszerekhez kapcsolódó paleofluidum-migráció az Óbányai-völgyben (Keleti-Mecsek)

Összefoglalás

Az elmúlt két évtizedben a Mecsek-hegység területén több triász és jura képződményben azonosítottak szénhidrogén-tartalmú paleofluidum-migrációra utaló nyomokat. Jelen tanulmány a legkeletebbi ismert előfordulást vizsgálja, amelyet a részben cementált törésrendszerek képviselnek az Óbányai-völgyben. Célunk ezen törésrendszerek kialakulási körülményeinek rekonstrukciója volt. Klasszikus szerkezetföldtani módszereket alkalmazva megkíséreltük azonosítani a repedésrendszert kialakító szerkezetfejlődési eseményeket. Eredményeink alapján két deformációs fázist azonosítottunk: a) egy redőképződést és b) egy ezt követő, balos eltolódást. A völgyben megfigyelt redőhöz kapcsolódó kőzetrések és vetők elméleti irányait meghatároztuk, majd ezeket összevetettük a terepi orientációs adatokkal. Elemzéseink alapján több, a redőződéshez kapcsolódó törési irányt, kalciteret és vetőbreccsát azonosítottunk. Hat érgeneráció fluidumzárvány-petrográfiai vizsgálata vizes és szénhidrogén-tartalmú fluidumzárványok jelenlétét igazolta. Eredményeink arra utalnak, hogy a szénhidrogén-tartalmú fluidummigráció a redőződéshez kapcsolódó négy elméleti törési sík egyikéhez kapcsolható. Noha a fluidumzárványok csupán korlátozott információt nyújtanak a fluidummigráció hőmérsékleti viszonyairól, több érszöveti sajátosság arra utal, hogy a törésrendszer fejlődése során a képződményben időszakosan megemelkedett fluidumnyomás uralkodott.

Tárgyszavak: szénhidrogén-migráció, breccsaér, tektonikus erek, redőződés, balos oldaleltolódás

Abstract

Over the past two decades, traces of hydrocarbon-bearing paleofluid migration have been detected in several Triassic and Jurassic formations in the Mecsek Mountains. This study focuses on the easternmost known hydrocarbon occurrence, represented by a partially cemented fracture network in the Óbánya Valley, with the aim of reconstructing the formation conditions of the fracture system. Classical structural geological methods were employed to characterize the evolution of this fracture system. As a result, two distinct deformation phases were identified: a) a folding event, and b) a subsequent left-lateral displacement. Theoretical orientation of fractures associated with the observed folds were determined and compared with field measurements. This approach allowed us to define several fault orientations and fault breccias, as well as to link calcite veins to a folding process. Fluid inclusion petrography revealed the presence of both aqueous and hydrocarbon-bearing fluid inclusions within six distinct vein generations. These findings suggest that hydrocarbon-bearing fluids migrated along one of the four deformation-related fracture sets in this fracture system. Although the nature of the fluid inclusion assemblages provides only limited constraints on the thermal conditions during fluid migration, several vein structures suggest episodic increases in fluid pressure during the system's evolution.

Keywords: hydrocarbon migration, breccia veins, tectonic veins, folding, sinistral strike-slip fault

Introduction

Fracture systems play a crucial role in subsurface fluid migration, influencing the movement of water, hydrocarbons, and other fluids (Moretti 1998, Nelson 2001). In sedimentary rocks, such as marls, fractures serve as high-permeability pathways, significantly enhancing fluid flow beyond what is achievable through primary porosity alone (Berkowitz 2002). However, it is essential to acknowledge the diverse range of fracture types – including cracks, fissures, joints and faults – whose fluid conductivity can vary to extreme degrees (Berkowitz 2002). Odling (1997) observed that joint systems composed of multiple, differently oriented sets often form well-connected networks, whereas fault systems, due to their density and orientation, tend to form one oriented network. Interestingly, such fracture sets can develop during progressive folding stages (Ramsay 1967), allowing enhanced fluid migration within the affected rock units. The mineralised fractures not only record the mechanisms of vein formation (Bons et al. 2012), but also provide valuable insights into the physicochemical conditions of paleofluid migration along fold-related fracture networks (Munz 2001, Fischer et al. 2009). Fischer et al. (2009) studied fracture-controlled paleofluid migration within a large-scale detachment fold in Mexico, using fluid inclusions in quartz and calcite veins. Their findings highlighted that even in extensively fractured formations, hydrologic systems can exhibit significant outcrop-scale heterogeneities, complicating the reconstruction of fluid migration events across broader areas. In the present study, understanding vein systems and fractures is essential for reconstructing the structural evolution and paleofluid migration in the study area.

Traces of hydrocarbon migration in fracture systems have been reported from several places in the Mecsek area over the past decade (e.g., Lukoczki et al. 2012, Han et al. 2022, Hrabovszki et al. 2023). The co-genetic occurrence of petroleum and aqueous fluid inclusions has not only allowed for the estimation of migration temperature but, in some cases, has also provided insights into the source rock of the petroleum-bearing fluids. Recently, Ladányi et al. (2023) reported that, in addition to the previously studied sites, Mesozoic formations in the northeastern segment of the Mecsek Mts. were also affected by hydrocarbon migration.

Here we present the results of a detailed structural analysis of the Óbánya Valley, with special regards to the calcite-cemented fracture system within the Komló Calcareous Marl Formation. Structural measurements, as well as petrographic and microanalytical methods were used to classify the calcite veins and establish, to the extent possible, the relative chronology of their formation. Furthermore, we correlated the identified fracture and vein generations with folding events recognised in the area (e.g., Püspöki et al. 2012). Lastly, we reconstructed the temporal relationship between petroleum-bearing fluid migration and the history of fracture formation and cementation in the study area.

Geological background

The study area is situated within the Tisza Mega-unit, which forms the southern segment of the Pannonian Basin. During the early stages of the Alpine orogenic cycle, the Tisza Mega-unit was positioned along the southern margin of the Eurasian continental plate, representing the northern shelf of the Tethys Ocean (Haas et al. 2012). As a result of regression, by the end of the Triassic, the marine environment gradually transitioned into freshwater conditions, leading to the deposition of fluvial, lacustrine, and marsh sediments at the Triassic–Jurassic boundary (Nagy 1969). During this period, coal deposits formed, which are characteristic lithological units in the Mecsek area. The proportion of fine-grained siliciclastic and carbonate sediments fluctuated in response to sea-level changes, resulting in the rhythmic alternation of spotted marl, calcareous marl, and argillaceous limestone. By the end of the Middle Jurassic, Mediterranean faunal elements began to appear and spread across the region due to the detachment of the Tisza Mega-unit from the European Plate (Géczy 1973, Vörös 1993). It is presumed that rifting, initiated during the Late Triassic, culminated in extensive alkaline basaltic magmatism during the Early Cretaceous. The resultant Late Mesozoic volcanic successions of the Mecsek Mountains form a dominant northeast-southwest trending belt approximately 250 km in length and 50 km in width (Bilik 1980, Kubovics et al. 1990, Harangi & Árváné-Sós 1993).

South of this volcanic zone lies the study area, the northeast-southwest trending Óbánya Valley, which holds geological interest because it exposes all the Jurassic formations of the Kisújbánya perisyncline. The valley runs parallel to the Döngölt Ditch, north of the Réka Valley. Near the village of Óbánya, the stratigraphic sequence predominantly consists of grey, spotted, bituminous, silty, and calcareous marl, along with clayey limestone. These deposits belong to the Toarcian–Bajocian Komló Calcareous Marl Formation (Böckh 1880, Hetényi 1966, Császár & Haas 1983, Galácz et al. 1992, Haas 1994, Némedi Varga 1998, Raucsik 2012). Further towards the village of Kisújbánya, the stratigraphy transitions into the Bathonian–Callovian Óbánya Limestone Formation, characterised by greenish, reddish, and grey marl, calcareous marl, and nodular limestone (Hetényi 1966, Császár & Haas 1983, Velledits et al. 1986, Galácz et al. 1992, Haas 1994, Némedi Varga 1998, Raucsik 2012). Continuing along the valley towards the village of Kisújbánya, the succession is dominated by the light-coloured, chert-bearing limestone of the Callovian–lower Kimmeridgian Fonyászó Limestone Formation, with a gradual decrease in chert content southwestward (Böckh 1880, Velledits et al. 1986). According to Galácz et al. (1992), carbonate rock sequences of Kimmeridgian–Tithonian age are present near Kisújbánya, classified as part of the Kisújbánya Limestone Formation (Haas 1994).

The structure of the Mecsek is characterised by complex anticline–syncline fold systems, with fold axes predominantly oriented northeast–southwest (Benkovics et al. 1997, CSONTOS et al. 2002). In the Máza-Dél–Váralja-Dél area, PÜSPÖKI et al. (2012) also observed folds with northeast–southwest-trending axes while investigating the Mecsek coal and the transgression-related thinning of coal sequences. These complex folds may have formed during the Cretaceous due to two distinct compression events, resulting in the development of east–west-trending folds (BERGERAT & CSONTOS 1988) and slightly asymmetric folds with northeast-southwest axes (NÉMEDI VARGA 1983, BERGERAT & CSONTOS 1988). Later, during the syn-rift phase of the development of the Pannonian Basin (~15 Ma), left-lateral transtensional movements (NÉMEDI VARGA 1983) led to the formation of pull-apart basins along the north and south boundaries of the mountain range (WEIN 1967, PETRIK 2009). The uplift of the Mecsek and Villány Mountains began in the early Pannonian (Late Miocene–Pliocene; FODOR et al. 1999; SEBE 2009, 2021; SZTANÓ & MAGYAR 2023; SEBE & PAZONYI 2025).

Methods

During the field surveys, orientation data of bedding planes as well as mineralised and unmineralised fractures were measured in the Óbánya Valley using a Freiberg compass and the FieldMove Clino mobile application. The collected data were graphically analysed using the Stereonet 11 software. After the macroscopic description of the collected hand specimens, 30-µm thin sections were prepared from seven samples. Microscopic petrographic observations were conducted using an Olympus SZX-7 polarising stereomicroscope, an Olympus BX-41 polarising microscope, and a Reliotron VII cathodoluminescence (CL) device mounted on an Olympus BX-43 microscope. To differentiate vein-forming carbonate phases, the thin sections were treated with acidic solutions of alizarin red S and potassium ferricyanide following the method of DICKSON (1965). The interpretation of carbonate staining was based on the findings of LINDHOLM & FINKELMAN (1972), where a pink colouration in calcite indicates an FeO content of ≤0.5%, classifying it as iron-free, whereas a blue coloration suggests an FeO content above this threshold, indicating iron-bearing calcite. UV-fluorescent petrography and microspectroscopic analyses were performed using a 100 W mercury vapour light source equipped with an Olympus U-MNU2 filter cube (excitation wavelength: 360–380 nm, dichroic filter: 400 nm, cutoff filter: 420 nm). Fluorescence spectra were recorded using an Ocean Insight (OceanOptics) QEPRO spectrometer connected to an Olympus BX-41 polarising microscope. Spectra were acquired from a 2 µm diameter spot with an 8 s acquisition time using the OceanView software and the data were normalised to their maximum intensity for comparability. To describe fluid inclusions, the terminology recommended by DIAMOND (2003) was followed. Microthermometric analysis of fluid inclusions was conducted using a Linkam MDS600 heating-freezing stage attached to an Olympus BX-41 polarising microscope. The system was calibrated with synthetic fluid inclusions in quartz at reference temperatures of –56.6 °C, 0.0 °C, and 374 °C. The vapour to liquid phase ratio of fluid inclusions was determined based on 2D microscopic images analysed with ImageJ 1.53 software and are expressed as vapour area% referring to the percent area of the vapour phase within a liquid-dominant fluid inclusion. Micro X-ray fluorescence (µXRF) mapping was carried out using a Horiba Jobin Yvon XGT-5000 X-ray fluorescence spectrometer, equipped with a Rh X-ray source operating at 30 kV and 0.5 mA. All analyses described above were conducted at the Department of Geology, University of Szeged.

Results

Field observations

Sampling was conducted at eight outcrops within the Óbánya Valley. The host rock of the studied vein samples (OB20/01–OB20/08) is primarily fine-grained marl with an earthy appearance, classified as part of the Komló Calcareous Marl Formation (*Figure 1*). The vein openings generally do not exceed 10 cm in width, while the vein-forming crystals display a parallel arrangement perpendicular to the vein walls, reaching a maximum length of approximately 3 cm. The tectonic veins of the Óbánya Valley predominantly consist of white and grey calcite crystals (*Figure 2A*).

During the field measurements, we recorded bedding planes and the orientation data of both filled and unfilled fractures, as presented in *Appendix 1* and *Appendix 2*, and summarised in *Table I*. In the valley area, calcite cemented fractures can be classified into four distinct orientation sets (*Figure 1B*). Near the Bodzás Spring, the dip directions of the bedding planes exhibit significant variation (*Figure 1B*). At outcrop OB20/06 and OB20/07, sedimentary layers and fractures cemented by calcite were observed. Near the Bodzás Spring, a fold with an axis orientation of 200°/18° was identified, consistent with preliminary exploration results (LADÁNYI 2021).

In three outcrops (OB20/01, OB20/05, OB20/08), calcite cementing the fractures consists of alternating grey and white zones, which are nearly parallel to each other and to the vein walls (*Figure 2A*). The grey calcite crystals range in size from 1 to 5 mm, whereas the white calcite grains vary between 0.2 and 3 cm.

Outcrop OB20/03 reveals breccia veins (*sensu* BONS 2000) consisting of white calcite cement and host rock fragments. Additionally, in this outcrop, calcite slickenfibres appear at the interface between the vein and the host rock over a section of nearly 40 cm (*Figure 2B*). The orientation of the fault plane is 332°/84°, and the pitch of the slickenfibres is 22° WSW, indicating a sinistral displacement (*Figure 2B*). Within the breccia vein, clasts frequently form larger, spherical clusters (*Figure 2C*). The clasts of the host rock consist of brownish, micritic marl with wackestone–packstone fabric containing abundant recrystallised radiolarians, bositria,

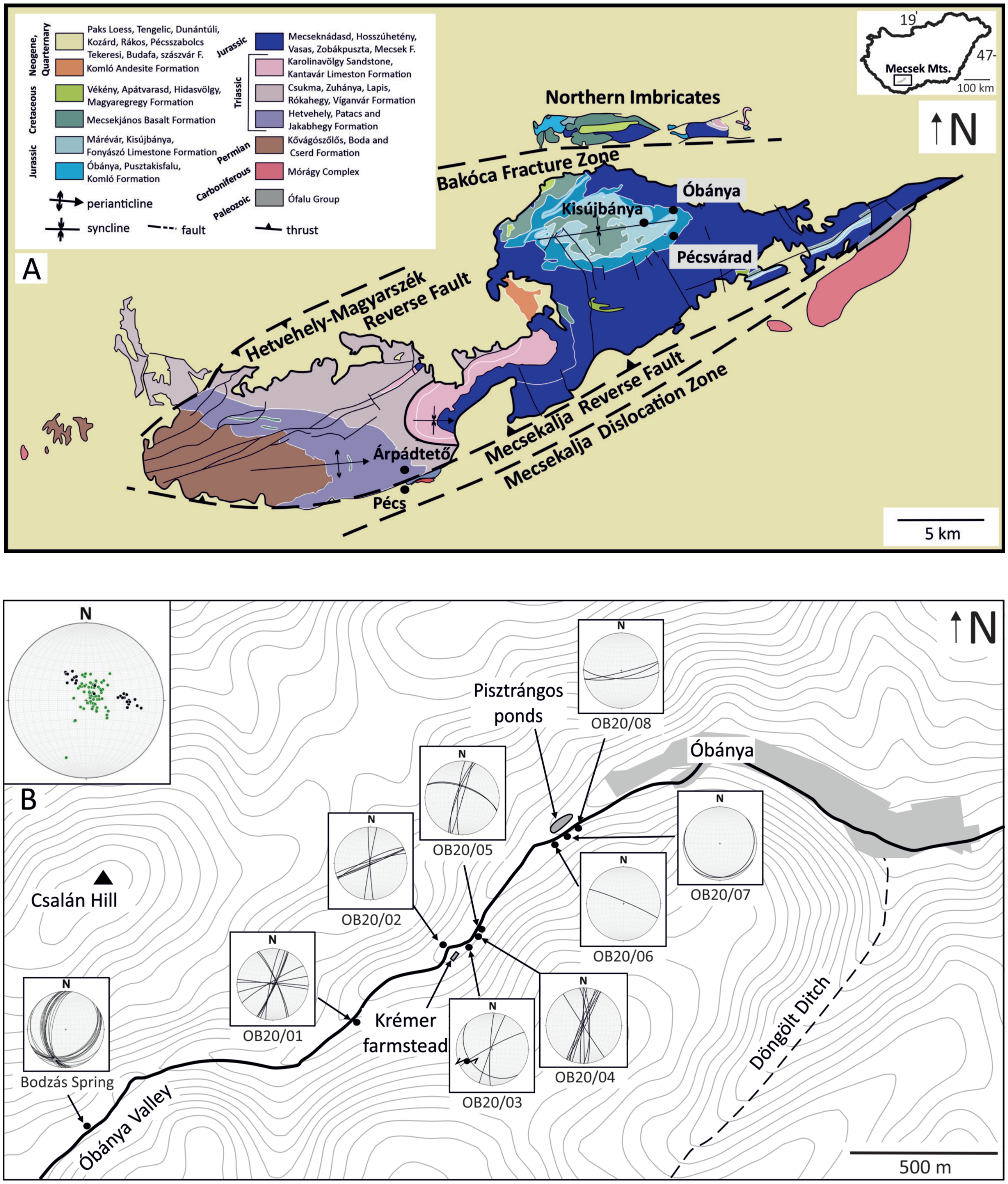

Figure 1. A) Geological map of the Mecsek Mountains (modified after KONRÁD et al. 2010). The red rectangle indicates the Óbánya Valley shown in Figure B. B) Sampling points in the Óbánya Valley. For the Bodzás Spring site, bedding planes are displayed on the stereogram, while calcite veins are indicated at the sampling points (OB20/01–OB20/08). The stereograms are lower hemisphere projections. The stereogram in the upper left corner shows the orientation data of bedding planes recorded in the valley, represented as pole points. Green points indicate measurements of bedding planes from the valley, while black points correspond to bedding planes measured at the Bodzás Spring.

1. ábra. *A) A Mecsek-hegység geológiai térképe (KONRÁD et al. 2010, módosítva). A piros téglalap a B ábrán látható Óbányai-völgyet jelöli. B) Mintavételi helyek az Óbányai-völgyben. A sztereogramok Schmidt-félgömbön, alsó vetítéssel készültek. A Bodzás-forrás esetében a sztereogramon a rétegsíkok vannak ábrázolva, míg a mintavételi helyek esetében (OB20/01–OB20/08) a kalciterek. A bal felső sztereogramon a völgy területén rögzített réteglapok orientációs adatai láthatók póluspontként ábrázolva. A zöld pontok a völgy teljes hosszán mért rétegeket, míg a fekete pontok a Bodzás-forrásnál mért rétegeket jelölik.*

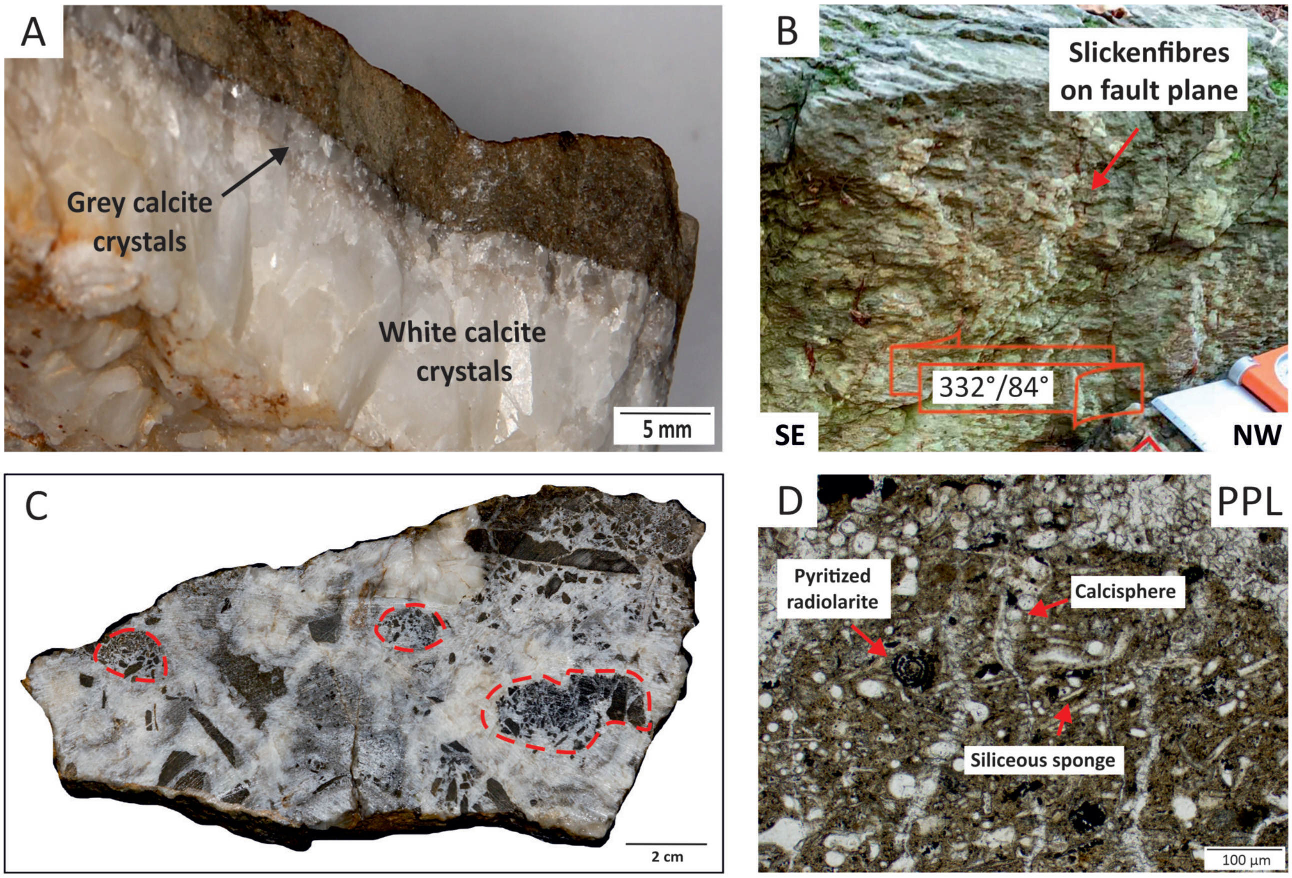

Figure 2. A) Nearly parallel white and grey calcite zones in sample OB20/01. B) A 30–40 cm long surface covered by calcite slickenfibres (sample site OB20/03). Red arrows indicate the direction of displacement on the fault plane, which has an orientation of 332°/84°. C) Angular wall rock clasts within the breccia vein (sample OB20/03), with red dashed lines marking the boundaries of the wall rock clasts. D) Recrystallised microfossils in the host rock (PPL – plane-polarised light). Red arrows highlight characteristic components of the host marl.

2. ábra. *A) Egymással közel párhuzamos lefutású, fehér és szürke színű kalcitzónák az OB20/01 mintában. B) 30–40 cm hosszú ásványlépcsőket tartalmazó vetősík (OB20/03 mintavételi hely). A piros nyilak az elmozdulás irányát jelölik, a vetősík orientációja 332°/84°. C) Szögletes mellékkőzetzárványok a breccsaérben (OB20/03 minta). A piros szaggatott vonalak a mellékkőzetzárvány-halmazok határát jelölik. D) A mellékkőzetben megjelenő, átkristályosodott mikrofosszíliák (1N felvétel).*

silica spicules, and calcite spherules. The radiolarians are frequently pyritised (*Figure 2D*). The spaces between the wall rock clasts are filled with white calcite, which also contains small (<1 cm) fragments of the host rock.

Vein petrography

In the Óbánya Valley, six vein generations have been identified based on the morphology of calcite crystals and the presence of host rock clasts. *Figure 3* displays the paragenetic sequence of these vein generations, and *Table I* summarises their microstructural characteristics. The six generations of calcite are presented in the established relative sequence.

Core-rim calcite vein type

The Cal_{CR} (core-rim) calcite vein generation consists of crystals with lighter inner (core) domains, ranging from 50 to 200 µm in diameter, and darker outer (rim) zones, measuring 100– 300 µm in width. This vein generation predominantly exhibits an NNE–SSW to ENE–WSW strike orientation (*Table I*). The blocky and occasionally elongate blocky crystals (*sensu* Bons 2000) display a gradual increase in size from the vein wall toward the centre, reaching up to 2.5 mm. Crystal growth is typically oriented toward the vein centre (*Figure 4A*). In some instances, the dark outer portions of the crystals contain multiple nucleation sites (*Figure 4B*). The core-rim domains are distinguishable under polarised light, cathodoluminescence (CL) and UV- fluorescence imaging (*Figure 4B, C*). Carbonate staining reveals a similar blue hue in both domains, suggesting that both the core and the rim consist of iron-rich calcite.

This vein generation exhibits macroscopic and microscopic deformation in samples OB20/06, OB20/07a, and OB20/07b (*Figure 4A*). Adjacent to the calcite veins, a dark brownish-grey zone is observed (*Figure 4A*). The crystals of Cal_{CR} terminate within this zone in euhedral shape, suggesting the formation of this dark zone postdating the Cal_{CR} vein generation. Micro-XRF mapping indicates that this dark zone has elevated aluminium and silicon content compared to the Cal_{CR} vein generation (*Figure 4D*). Unlike the host rock, the phase with elevated aluminium and silicon content lacks microfossils but is characterised by laminated structure.

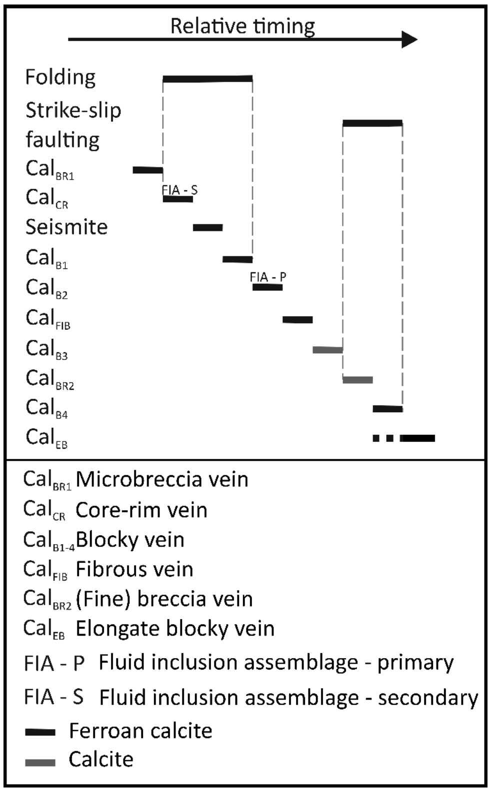

Figure 3. Deformation and cementation events and their inferred relative sequence in the Óbánya Valley. The individual lines represent the relative timing of vein generations. Due to the absence of cross-cutting relationships, the temporal position of the Cal_{EB} vein generation remains uncertain. FIA-P represents primary, whereas FIA-S refers to secondary hydrocarbon-bearing fluid inclusion assemblages. The vertical dashed lines indicate the vein generations affected by folding and left-lateral strike-slip displacement.

3. ábra. *Az Óbányai-völgyben azonosított deformációs és cementációs események feltételezett relatív sorrendje. Az egyes vonalak az érgenerációk egymáshoz viszonyított időbeli viszonyát jelölik. A Cal_{EB} érgeneráció időbeli elhelyezkedése metsződési viszonyok hiányában bizonytalan. Az FIA-P az elsődleges genetikájú, míg az FIA-S a másodlagos genetikájú, szénhidrogén-tartalmú zárványegyütteseket jelöli. A függőleges szaggatott vonalak a redőződés és a balos oldaleltolódás által érintett érgenerációkat jelzik.*

Breccia vein type I (Cal_{BR1})

In the studied area of the valley, two breccia vein generations (Cal_{BR1} and Cal_{BR2}) were distinguished based on clast size and the iron content of the cementing calcite. One of the breccia vein generations, Cal_{BR1}, is characterized by iron-rich calcite with a blocky texture (*Figure 5*). The Cal_{BR1} vein generation is only observable at microscopic scale, and its orientation remains unknown, but most vein generations intersect this vein generation (*Figure 5*). The calcite crystal size reaches approximately 200 µm, while the clasts derived from the host rock range from 0.1 to 1 mm in length. The clasts exhibit both angular and rounded morphologies. The Cal_{BR2} vein will be presented later.

Blocky calcite vein type

Calcite veins exhibiting blocky textures (Cal_{B1-4}) are oriented NNE–SSW and ENE–WSW (*Table I*). Four generations of Cal_B were identified, distinguished by the iron content and orientation of the calcite (*Figure 3*). These veins consist of multiple subparallel zones (*Figure 6A*), with boundaries marked by bands of host rock inclusions ≤50 µm in size (*Figure 6A*). The outermost zone consists of calcite crystals ≤100 µm in diameter, followed inward by a zone of blocky calcite crystals that progressively increase in size towards the vein centre (*Figure 6A*). Within the inner part of the vein, the blocky grains reach sizes up to 6 mm. Carbonate staining reveals two distinct calcite zones with differing iron contents, alternating within the vein (*Figure 6A*). The calcite crystals in both the iron-free and the iron-rich zones exhibit syntaxial growth morphology, indicating that the crystal growth initiated from the vein walls and progressed toward the centre (BONS 2000, BONS et al. 2012). The alternation of iron-free and iron-rich zones suggests a change in fluid chemistry during vein crystallisation. Therefore, the zones shown in *Figure 6A* may have formed during multiple precipitation phases. Regardless of iron content, type I and type II deformation twins (*sensu* BURKHARD 1993; FERILL et al. 2004) are observed in the calcite crystals (*Figure 6A, B*). Some calcite grains display growth zonation, marked by solid inclusions of the host rock trapped along zone boundaries (*Figure 6B*). The growth direction of calcite crystals and zonation patterns are highlighted in CL images (Figure 6C), where variations in CL activity distinguish the different zones.

Fibrous calcite vein type

Similar to the Cal_{BR1} vein generation, the Cal_{FIB} vein generation can only be observed at microscopic scale, and its orientation is not known, but it intersects most generations of veins. The Cal_{FIB} veins consist of fibrous calcite crystals that are oriented perpendicular to the vein wall and parallel to each other (*Figure 4*). These veins are typically ≤2 mm thick and often occur in subparallel arrangement.

Based on observations from samples OB20/07a and OB20/07b, veins of this generation are approximately perpendicular to, and frequently intersect the Cal_{BR1}, Cal_B, and Cal_{CR} vein generations (*Figure 5*). The calcite fibres range from 0.1 to 1.5 mm in length, and in most cases, they grow toward the vein wall (*Figure 5*). Carbonate staining indicates that the Cal_{FIB} veins are composed of iron-rich calcite.

Breccia vein type II (Cal_{BR2})

The second breccia generation (Cal_{BR2}) predominantly exhibits a NE–SW strike orientation (*Table I*). Calcite crystals within Cal_{BR2} veins display a blocky texture (*Figure 7A*) and range in size from 50 µm to 3 mm. The clasts have both rounded and angular morphologies. Clast clusters, enclosed by inclusion-free calcite cement, can reach up to 4 mm in size (*Figure 7A, B*); however, certain areas contain fine-grained fragments (≤50 µm) as well.

Occasional type I, II, and IV deformation twins (*sensu* BURKHARD 1993) are observed in the calcite grains (*Figure 7A, C*). In some regions, calcite crystals display growth zonation, with zone boundaries marked by solid inclusions of the host rock (*Figure 7C*). Among the host rock clasts and the

Table I. Summary of the texture, orientation and characteristics of the fluid inclusions in the studied vein phases. The stereograms show the orientations specific to a given vein generation in black, while the four fracture planes associated with the observed fold are indicated in red (TWISS & MOORES 1992). The stereograms were created using a lower hemisphere projection. PPL – plane-polarised light; N.d. – no data; FIA – fluid inclusion assemblage.

***I. táblázat.** Az ércementek szövetének, orientációjának és a bennük található fluidumzárványok jellemzőinek összefoglalása. A sztereogramokon szereplő fekete főkörök az adott érgenerációra jellemző orientációkat reprezentálják, míg a piros szín a redőződéshez kapcsolható négy törési síkot jelöli (TWISS & MOORES 1992). A sztereogramok Schmidt-félgömbön, alsó vetítéssel készültek. PPL – párhuzamosan polarizált fény; N.d. – nincs adat; FIA – fluidumzárvány-együttes.*

Veins	Typical vein orientations	Fluid inclusions assemblages (FIAs)	Cement mineralogy and crosscutting relations
Core-rim vein (Cal_{CR})	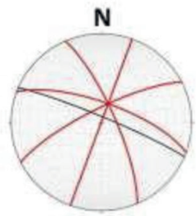	Secondary hydrocarbon FIA PPL: yellowish-brownish colour UV: yellow/blue fluorescence colour Size: ≤ 3 μm Vapour area% = 10–20	Ferroan calcite
Microbreccia vein (Cal_{BR1})	N.d.	N.d.	Ferroan calcite
Blocky vein (Cal_{B1-4})	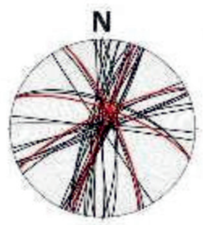	Primary FIA PPL: yellowish-brownish colour; dark brownish colour UV: yellow/blue fluorescence colour; red fluorescent colour Size: ≤ 5 μm (yellow/blue); 8–12 μm (red) Vapour area% = 10–20 (yellow/blue); 50–90 (red)	Ferroan calcite
		Secondary FIA PPL: yellowish-brownish colour; reddish-brownish colour UV: yellow fluorescence colour; red fluorescence colour Size: ≤ 3 μm (yellow); >8 μm (red) Vapour area% = 10–30 (yellow); 60–90 (red) Th= 58–101 ºC (n=11)	Ferroan calcite; crosscut Cal_{CR}
		N.d.	Calcite
Fibrous vein (Cal_{FIB})	N.d.	N.d.	Ferroan calcite; crosscut Cal_{BR1} and Cal_{B1-2}
Fine breccia vein (Cal_{BR2})	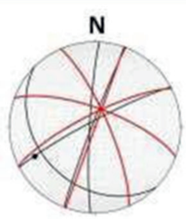	Secondary FIA PPL: colourless Size: 2–5 μm	Calcite; crosscut Cal_{B1-3}
		Secondary FIA PPL: colourless Size: ≤ 5 μm Vapour area% = 10–30	
Elongate blocky vein (Cal_{EB})	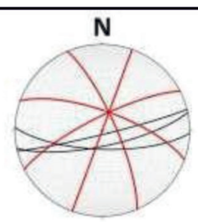	N.d.	Ferroan calcite

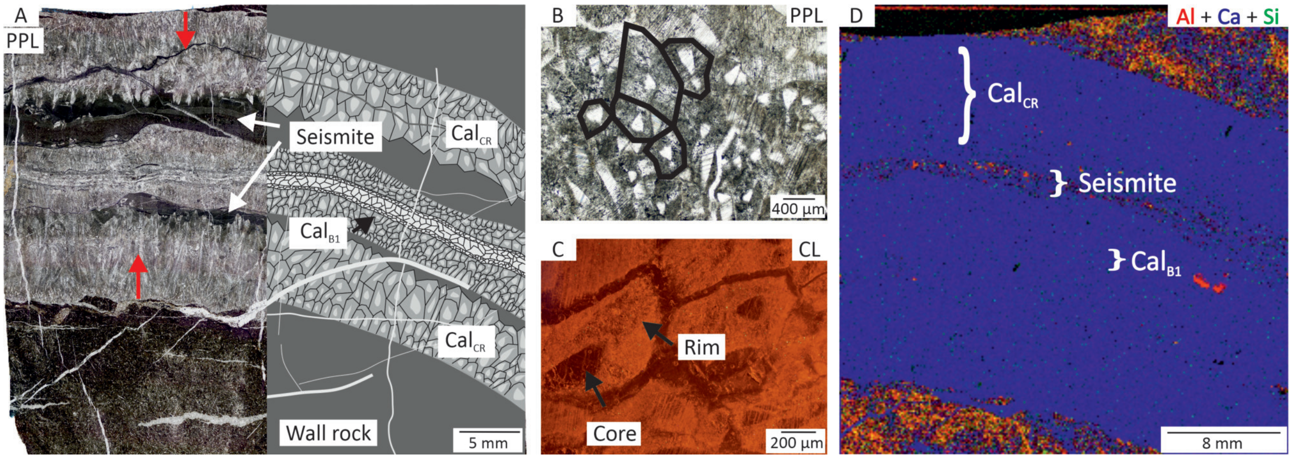

Figure 4. A) The folded Cal$_{CR}$ and Cal$_{B}$ vein generations, as well as the "seismite" in PPL images. The Cal$_{B}$ vein generation intersects the Cal$_{CR}$ vein generation at different orientations. Red arrows indicate the growth direction of calcite grains. A schematic figure of the different vein generations is shown on the right side of the figure. B) Multiple nuclei are observed in the periphery of the calcite grains forming the vein. The black line marks the boundary of the rims (thus, the grains). C) The core-rim structure in CL. D) Representative elemental distribution from Figure A. Differences in Al, Ca, and Si composition distinguishes the Cal$_{CR}$ and the Cal$_{B1}$ vein generations from the seismite zone. PPL – plane-polarised light; CL – cathodoluminescence.

4. ábra. *A) A redőződött Cal$_{CR}$ és Cal$_{B}$ érgenerációk, valamint a közöttük elhelyezkedő szeizmit 1N felvételen. A Cal$_{B}$ érgeneráció eltérő orientációkban metszi a Cal$_{CR}$ érgenerációt. A piros nyilak a kalcitszemcsék növekedési irányát jelölik. Az ábra jobb oldalán a minta sematikus ábrázolása látható. B) Az éralkotó kalcitszemcsék peremi részein belül helyenként több mag figyelhető meg (1N felvétel). A fekete vonal a peremek, azaz a szemcsék határát jelöli. C) A mag-perem szerkezet CL-felvételen. D) Mikro-XRF-elemtérkép az A) ábrán bemutatott területről. Az Al, Ca és Si elemtérképek kijelölik a Cal$_{CR}$ és a Cal$_{B1}$ érgenerációk, valamint a szeizmit zóna határait. CL – katód-lumineszcencia.*

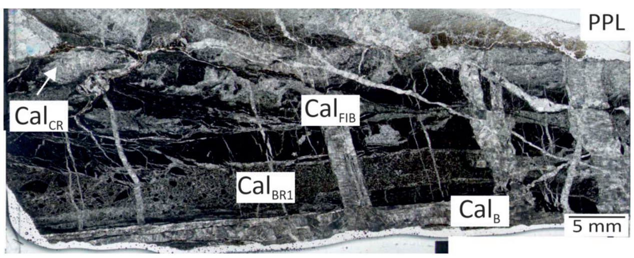

← **Figure 5.** In the OB20/07b sample contains the Cal$_{CR}$, Cal$_{B}$, Cal$_{FIB}$, and Cal$_{BR1}$ vein generations. Based on crosscutting relationships, Cal$_{BR1}$ is considered one of the earliest vein-forming events in the area, whereas Cal$_{FIB}$ is likely among the youngest vein generations. PPL – plane-polarised light.

← ***5. ábra.*** *Az OB20/07b mintában a Cal$_{CR}$, Cal$_{B}$, Cal$_{FIB}$ és Cal$_{BR1}$ érgenerációk azonosíthatók (1N felvétel). A metsződési viszonyok alapján a Cal$_{BR1}$ a terület egyik legidősebb érgenerációjának tekinthető, míg a Cal$_{FIB}$ feltehetően az egyik legfiatalabb érgeneráció.*

calcite grains cementing the fracture, fragments appearing to be older calcite veins are also present (*Figure 7A*). These vein fragments consist of multiple parallel zones that are sharply separated from each other by host rock clasts. Carbonate staining reveals that the calcite cement forming the Cal$_{BR2}$ vein generation is iron-free, whereas the older vein fragments consist of iron-rich calcite (*Figure 7D*).

Elongate blocky calcite vein type

Along the valley, a calcite vein generation composed of elongate blocky crystals (Cal$_{EB}$) follows a WSW–ENE strike (*Table I*). Similar to the Cal$_{B}$ veins, these veins are composed of subparallel zones, separated by bands of host rock inclusions at their boundaries (*Figure 8*). Fine-grained calcite

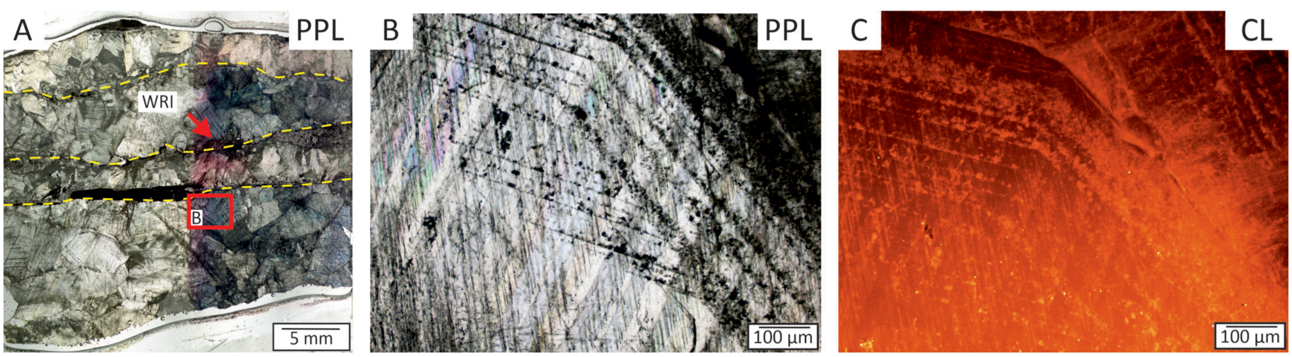

Figure 6. Typical texture of the Cal$_{B}$ vein generation in PPL. A) The boundaries of the parallel zones are marked by wall rock inclusions (WRI). The blue and pink colours indicate alternating bands of iron-rich and iron-free calcite observed based on carbonate staining. The yellow dashed line marks the boundaries of the zones. B) Growth zones marked by wall rock inclusions. C) CL image of B showing the wall rock inclusion planes.

6. ábra. *A Cal$_{B}$ érgeneráció jellemző szövete 1N felvételen. A) Az egymással párhuzamos zónák határát mellékkőzetzárványok (WRI) jelölik ki. Karbonátfestés alapján a kék szín a vasas, míg a rózsaszín a vasmentes kalcit jelenlétét mutatja. A sárga szaggatott vonal a zónák határát jelöli. B) Mellékkőzetzárványok által kijelölt növekedési zónák. C) A B) ábrán látható mellékkőzetzárvány-síkok CL-felvételen.*

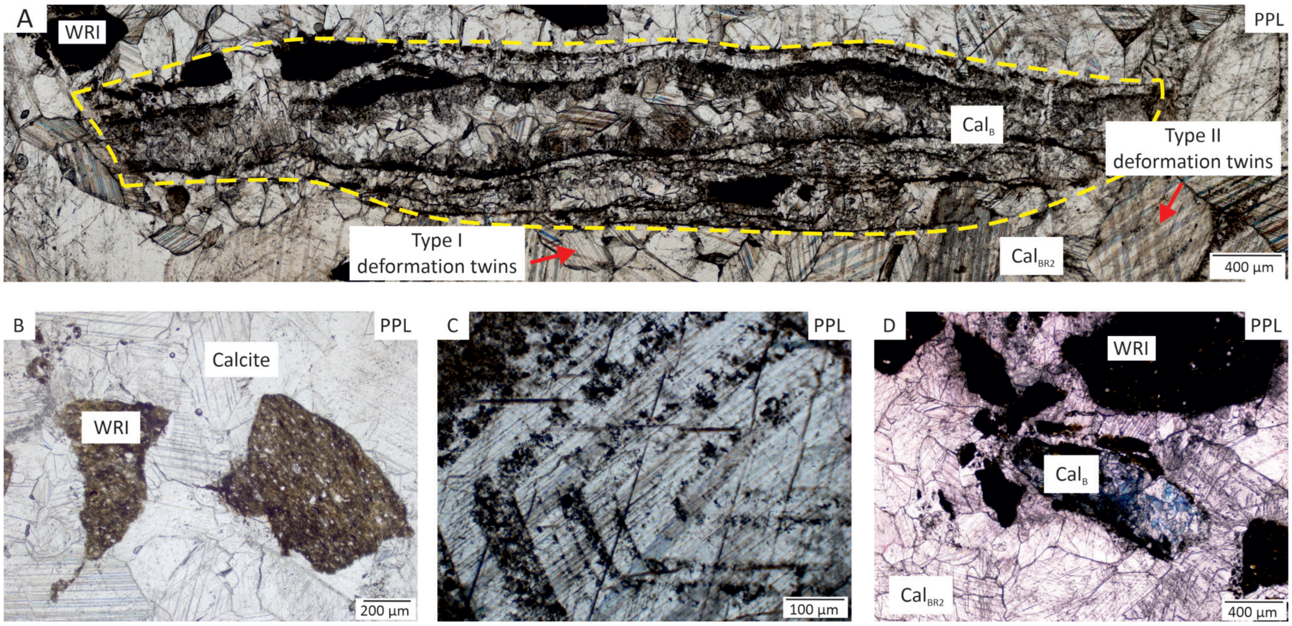

Figure 7. Typical texture of the Cal$_{BR2}$ vein generation in PPL. A) Type I and II deformation twins in blocky calcite grains. A fragment of an older vein is observed within a Cal$_{BR2}$ calcite vein. The yellow dashed line marks the boundary of the vein fragment. B) Larger clasts of host rock enclosed in the calcite vein. C) Wall rock inclusions situated in the growth zones of the grains. D) Detail of the Cal$_{BR2}$ vein after carbonate staining. The blue areas indicate the presence of iron-rich calcite, while the pink areas indicate iron-free calcite. WRI – wall rock inclusion; PPL – plane-polarised light.

7. ábra. *A Cal$_{BR2}$ érgeneráció jellemző szövete 1N felvételeken. Az A) ábrán I. és II. típusú deformációs ikrek láthatók tömbös kalcitszemcséken. A nagyobb méretű kalcitszemcsék között egy idősebb ér töredéke figyelhető meg. A sárga szaggatott vonal az értöredék határát jelöli. B) Nagyobb méretű mellékkőzetklasztok kalcitszemcsék között (1N felvétel). C) A szemcsék növekedési zónáit mellékkőzetből származó zárványok jelzik (1N felvétel). D) A Cal$_{BR2}$ ér részlete karbonátfestést követően. A kék részek vasas, míg a rózsaszín részek vasmentes kalcit jelenlétét igazolják. WRI – mellékkőzetzárvány.*

crystals (<50 µm) are oriented nearly perpendicular to the vein walls, classified as loser grains (Bons 2000). In contrast, some crystals widen toward the vein centre, reaching lengths up to 1 mm, corresponding to winner grains (Bons 2000; *Figure 8*). Carbonate staining confirms that all zones within the vein are composed of iron-rich calcite.

Fluid inclusion petrography

Fluid inclusion assemblages (FIAs) of both primary and secondary origin are observed in the Cal$_{CR}$, Cal$_{B}$, Cal$_{BR1}$ and Cal$_{BR2}$ vein generations. Fluid inclusions are classified into types based on their colour, UV fluorescence characteristics and type of phases – liquid (L) or vapour (V) – they contain (*Table II*).

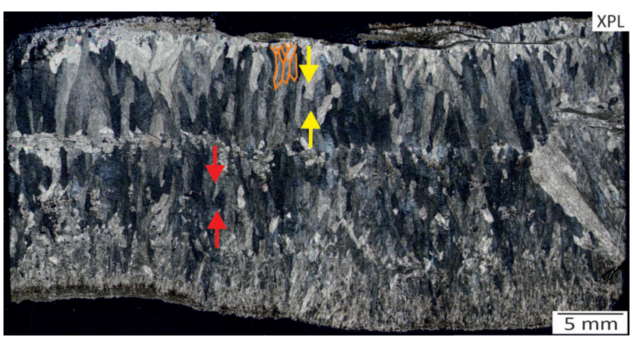

Figure 8. Elongate blocky calcite crystals in the Cal$_{EB}$ vein generation. The orange line indicates the grain boundaries, while the red and yellow arrows indicate the direction of crystal growth. XPL – cross-polarised light.

8. ábra. *Megnyúlt, tömbös kalcitkristályok a Cal$_{EB}$ érgenerációban (+N felvétel). A narancssárga vonal a szemcsék határát, míg a piros és sárga nyilak a szemcsék növekedési irányát jelölik.*

The aqueous fluid inclusions were classified into two groups based on the type of phases present: liquid (L) and liquid+vapour (L+V). Liquid fluid inclusions occur within Cal$_{B}$, the peripheral zone of Cal$_{CR}$, as well as in the Cal$_{BR1}$ and Cal$_{BR2}$ vein generations (*Figure 9A, B*). These inclusions, typically ranging from 2 to 5 µm in size, exhibit elongate, round, or rectangular morphologies. They appear colourless under normal light and show no fluorescence under UV illumination. The inclusions are commonly arranged in planes oriented obliquely with respect to the calcite crystal boundaries, with multiple intersecting planes within the same crystal. In the Cal$_{BR2}$ vein generation, a small number of L+V fluid inclusions are also present alongside the dominant liquid inclusions. These L+V inclusions, ≤5 µm in size, similarly appear colourless under normal light and lack fluorescence under UV illumination. They are arranged in planes that are not parallel to crystal boundaries or vein walls, suggesting a secondary origin for both the liquid and liquid + vapour inclusions. The vapour area% of the L+V fluid inclusions varies between 10 and 30%.

Hydrocarbon-bearing fluid inclusions can be classified as primary (FIA-P) or secondary (FIA-S) according to their genetic origin. The Cal$_{B}$ vein generation hosts primary, liquid + vapour fluid inclusions with irregular morphologies, classified into distinct FIAs based on their spatial distribution. Multiple parallel planes, typically observed along the

Table II. Summary of selected fluid inclusion parameters. FIA-AQ – aqueous fluid inclusion assemblage; FIA-P – primary fluid inclusion assemblage; FIA-S – secondary fluid inclusion assemblage; L - liquid; V - vapour; n.d. – no data; N.A. – not applicable.

II. táblázat. *A fluidumzárványok egyes paramétereinek részletes bemutatása táblázat formájában. FIA - AQ – vizes fluidumzárvány-együttes; FIA-P – elsődleges fluidumzárvány-együttes; FIA-S – másodlagos fluidumzárvány-együttes; L – folyadék; V – gőz; n.d. – nincs adat; N.A. – nem releváns.*

	FIA-AQ		FIA-P		FIA-S	
Liquid	water		hydrocarbon			
Genetics	secondary		primary		secondary	
Phases	L	L+V	L+V	L+V	L+V	L+V
Size (µm)	2–5	≤5	≤5	8–12	≤3	>8
PPL	colourless	colourless	yellowish-brown	brownish-reddish	yellowish-brown	brownish-reddish
UV	colourless	colourless	yellow or blue	red	yellow or blue	red
Vapour area%	0	10–30	10–20	50–90	10–30	60–90
T_h (°C) (L+V→L)	N.A.	n.d.	n.d.	n.d.	58–101	n.d.
Vein generation	Cal_B Cal_{CR} Cal_{BR1} Cal_{BR2}	Cal_{CR} Cal_{BR2}	Cal_B	Cal_B	Cal_B Cal_{CR}	Cal_B

vein walls, contain inclusions of varying size and colour (*Figure 10A*). Numerous fluid inclusions smaller than 5 µm are present, with a fluid phase exhibiting a pale yellowish-brown colour under transmitted light (*Figure 10A*). Under UV illumination, these inclusions display yellow or blue fluorescence (*Figure 10B*). The vapour area% of these inclusions ranges between 10 and 20%**,** regardless of fluorescence colour. Few fluid inclusions occur within the FIA, whose fluid phase appears dark brownish-reddish under transmitted light. These inclusions, typically 8–12 µm in size, exhibit reddish fluorescence under UV illumination (*Figure 10B*), with a vapour area% varying between 50 and 90%.

In both the Cal_B and Cal_{CR} vein generations, these hydrocarbon-bearing FIAs are typically arranged in planes that intersect calcite grain boundaries, indicating their secondary origin (FIA-S) (*Figure 10C, D*). Due to their small size, primary fluid inclusions within the Cal_B vein generation were unsuitable for homogenisation temperature measurements;

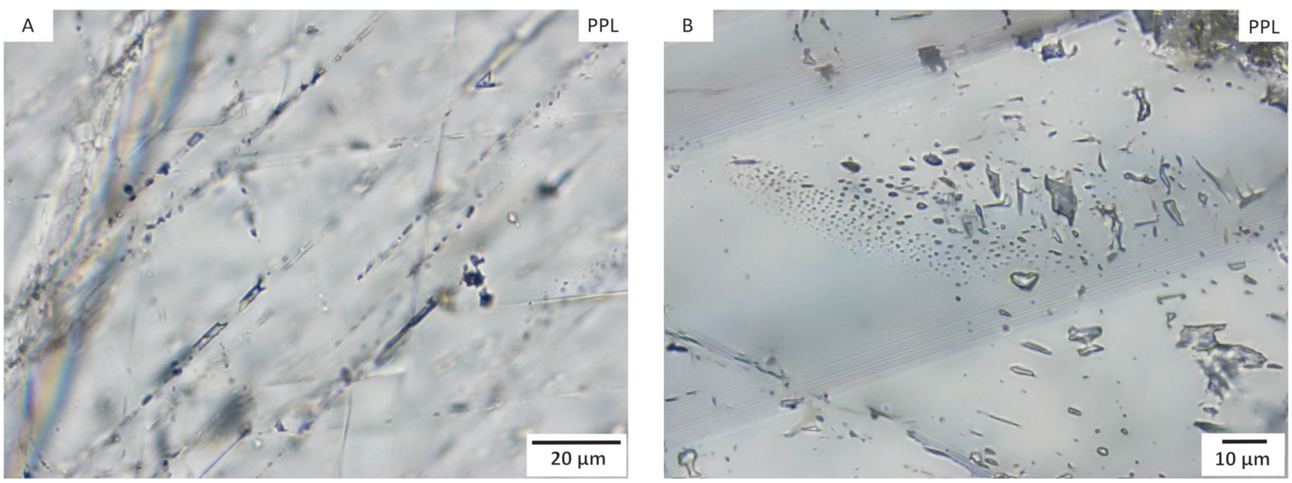

Figure 9. Fluid inclusions in the Cal_{BR2} vein generation. A) Liquid-phase inclusion planes running parallel to each other. B) Elongate, round, and rectangular fluid inclusions taken as composite photo of an extended depth of field. PPL – plane-polarised light.

9. ábra. *Fluidumzárványok a Cal_{BR2} érgenerációban 1N felvételeken. A) Egymással párhuzamos lefutású, fluidumzárványokból álló síkok. B) Megnyúlt, lekerekített téglalap alakú fluidumzárványok kiterjesztett mélységélességű, kompozit felvételen.*

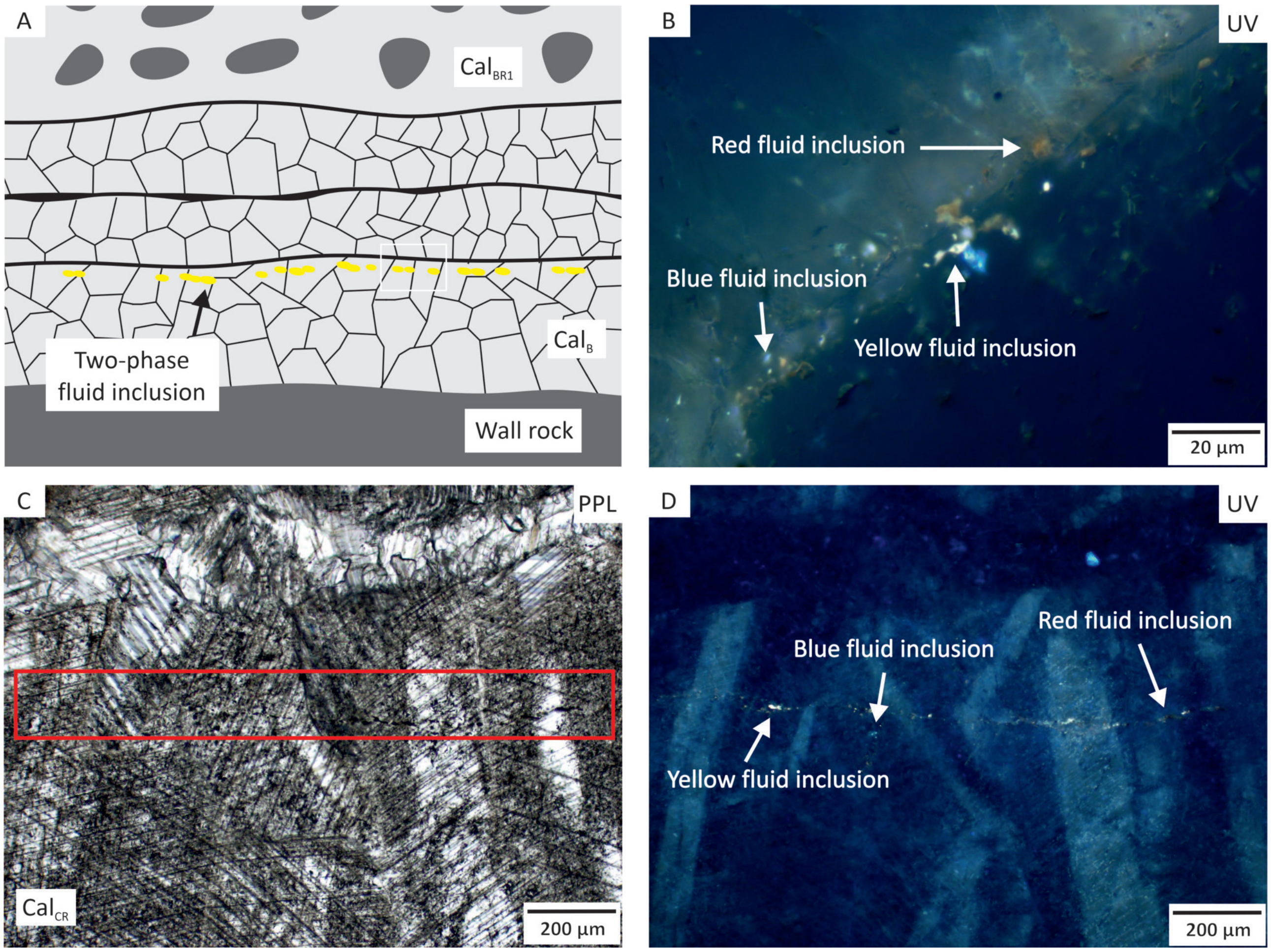

Figure 10. A) Schematic representation of a fluid inclusion assemblage (yellow) parallel to the vein wall in the Cal_B vein generation. The white rectangle delineates the location of the texture shown in Figure B. Liquid + vapour phase fluid inclusions of different colours under UV light in the Cal_B vein generation. C) A fluid inclusion band highlighted by the red rectangle crosscuts the grains of the Cal_{CR} vein generation. D) The same area as in C) under UV light, showing predominantly yellow-fluorescing fluid inclusions. Under UV illumination, the core and rim regions of the crystals in this vein generation exhibit different shades of blue. PPL – plane-polarised light.

10. ábra. *A) Sematikus ábra a Cal_B érgenerációban megjelenő, érfallal párhuzamos fluidumzárvány-együttesről (1N felvétel). A fehér téglalap a B ábra szöveti helyzetét jelöli. B) Folyadék-gőz fázisú, különböző színű fluidumzárványok UV-fény alatt a Cal_B érgenerációban. C) A piros téglalappal jelölt fluidumzárványsáv elmetszi a Cal_{CR} érgeneráció szemcséit. D) A C) ábrán látható terület UV-fény alatt, ahol túlnyomórészt sárgán fluoreszkáló fluidumzárványok figyelhetők meg. UV-gerjesztés hatására az ezen érgenerációhoz tartozó szemcsék magja és peremi része eltérő árnyalatú kék fluoreszcenciát mutat.*

however, secondary fluid inclusions (n = 11) yielded T_h(L+V L) values ranging from 58 to 101 °C (*Figure 11*). In the other FIAs the fluid inclusions were too small to be suitable for microthermometric measurements.

UV-fluorescence microspectroscopy was performed on primary, hydrocarbon-bearing fluid inclusions (FIA-P) in samples OB20/07a and OB20/07b from the Cal_{B2} vein generation. In these samples, a single plane hosts an assemblage of inclusions displaying three visually distinct fluorescence colours (*Figure 10B*). The maximum fluorescence intensity wavelength (λ_{max}) for the yellow-fluorescent inclusions at the vein margin is 535–536 nm, while the blue-fluorescent inclusions exhibit values ranging from 485 to 521 nm. The red-fluorescent inclusions show λ_{max} values between 554 and 644 nm (*Figure 12*).

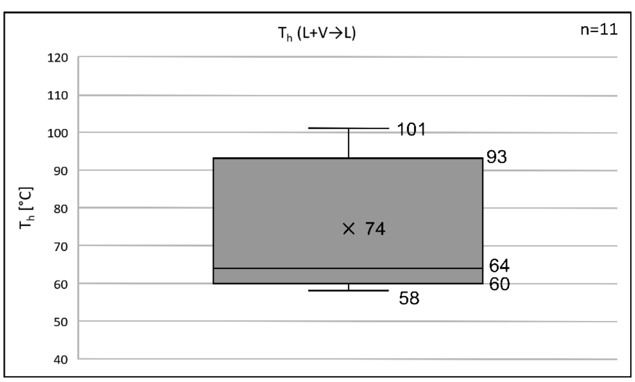

← **Figure 11.** Temperatures of homogenization (T_h) of the gas phase into the liquid phase determined by microthermometric measurements of secondary fluid inclusions exhibiting yellow fluorescence. In the diagram, the box represents the first and third quartiles of the dataset, while the "X" and the horizontal line within the box indicate the mean and median values.

← ***11. ábra.*** *A másodlagos genetikájú, sárga fluoreszcenciát mutató, a folyadékfázisba homogenizálódó fluidumzárványok homogenizációs hőmérsékletei (T_h). A diagramokon az interkvartilis terület a minta első és harmadik kvartilisét ábrázolja, míg az "X" és az interkvartilis területen belüli vízszintes vonal az átlagértéket és a mediánt jelöli.*

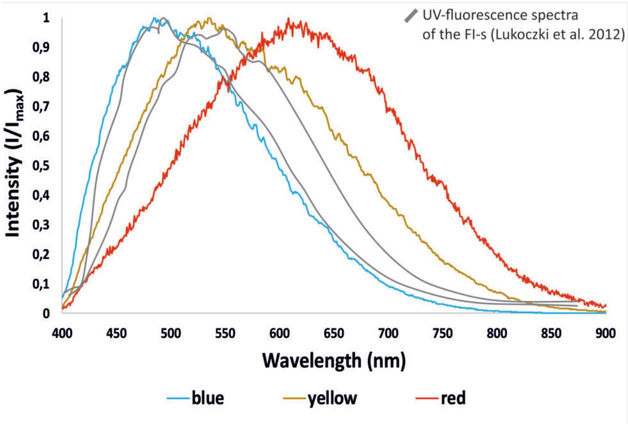

Figure 12. Characteristic spectra of fluid inclusion assemblages exhibiting three different fluorescence colours in sample OB20/07b. The grey curves represent the characteristic UV spectra of hydrocarbon-bearing fluid inclusions described by LUKOCZKI et al. (2012).

12. ábra. *A három különböző fluoreszcens színű fluidumzárvány-együttes jellemző spektruma az OB20/07b mintákban. A szürke görbék LUKOCZKI et al. (2012) által leírt, szénhidrogén-tartalmú fluidumzárványok jellemző UV-fluoreszcens spektrumait jelölik.*

Discussion

Traces of folding and brittle deformation

At Bodzás Spring, the strata on either side of the stream exhibit significantly different dip directions (*Appendix 1*), resulting in a cylindrical fold geometry, with an axis of 200°/18° (LADÁNYI 2021). Fractures can form within folds in four distinct orientations, each associated with the folding process (e.g., RAMSAY 1967, TWISS & MOORES 1992, DAVIS et al. 2011, FOSSEN 2016). One of these planes is parallel to the fold axial plane, while another is perpendicular to it, creating an intermediate spacing pattern within the folded layers. The remaining two planes typically form a conjugate pair, with each plane intersecting the one perpendicular to the fold axial plane at an acute angle (*Figure 13A, B*). Most of the fractures observed in the valley align closely with these four characteristic fracture planes of the fold (*Table I*). Based on these observations, the orientation of the calcite vein generations Cal_{CR}, $Cal_{B1–4}$, and Cal_{BR2} can be attributed

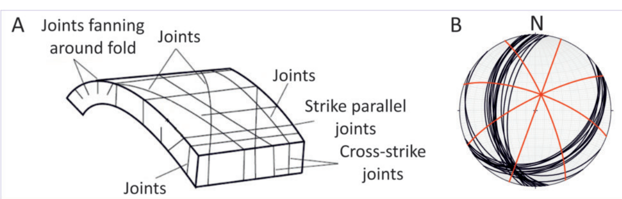

Figure 13. A) Fracture systems and conjugate fault pairs that develop on fold limbs (modified after VAN DER PLUIJM & MARSHAK 2004). B) The orientation data of bedding planes measured near Bodzás Spring (black lines) and the four theoretical fracture planes related to folding (red lines) are plotted on the stereogram. The stereographic projection was drawn on Smidt net, lower hemisphere.

13. ábra. *A) Redőszárnyakon kialakuló kőzetrésrendszerek és konjugált vetőpárok (VAN DER PLUIJM & MARSHAK 2004, módosítva). B) A Bodzás-forrás közelében mért réteglapok orientációs adatai (fekete főkörök) és a redőződéshez kapcsolódó négy elméleti törési sík sztereogramon ábrázolva. A sztereogram Schmidt-félgömbön, alsó vetítéssel készült.*

to fracture systems related to the folding process in the vicinity of Bodzás Spring (*Table I*).

At sampling sites OB20/06 and OB20/07, calcite veins underwent micro-scale folding along with the host rock. These deformed veins belong to the Cal_{B1} and Cal_{CR} vein generations (*Figure 4A*). The deformation of the veins indicates that they formed either prior to or synchronously with folding, classifying them as pre- or synkinematic relative to the folding event. Adjacent to the calcite veins, a dark brownish-grey zone is observed, which is folded (*Figure 4A*). This type of fracture filling was referred to as a “seismite” by SEILACHER (1969) and may form during seismic events when fractured host rocks liquefy and intrude into open fractures (LUNINA 2019).

At outcrop OB20/03 (*Figure 1B*), a vertical fault plane covered by calcite slickenfibres preserves evidence of sinistral strike-slip faulting (*Figure 2B*). Along this mineralised surface, a breccia vein is present (*Figure 2B*). Microscopic examination of this Cal_{BR2} vein generation reveals the presence of older, fragmented vein material alongside host rock clasts (*Figure 7A*). It is inferred that during the sinistral displacement, not only host rock fragments, but also vein fragments may have become detached and transported away from the vein wall. These displaced vein fragments are composed of iron-rich calcite crystals, as indicated by carbonate staining. The crystals exhibit syntaxial growth nearly perpendicular to the vein wall, widening progressively toward the vein interior. Notably, these vein fragments lack hydrocarbon-bearing fluid inclusions, suggesting that this hydrocarbon-free fluid migration preceded the sinistral displacement, and resulted in the precipitation of iron-rich calcite crystals. These iron-rich crystals are likely associated with the Cal_{B1} vein generation.

The Cal_{FIB} and Cal_{BR1} vein generations cannot be precisely oriented within the structural framework. Consequently, their relative timing can only be inferred through microscopic crosscutting relationships, which suggest that both veins predate the sinistral displacement. However, based on crosscutting relationships, Cal_{BR1} veins formed prior to the $Cal_{B1–4}$ vein generations, while the Cal_{FIB} veins postdate the Cal_{B2} vein generation (*Figure 5A, Figure 3*).

The orientation of the Cal_{EB} vein generation does not correlate with the theoretical fracture sets associated with folding (*Table I*). These observations suggest that the formation of the Cal_{EB} veins must be unrelated to the folding process. Furthermore, crosscutting relationships between the Cal_{EB} veins and other vein generations are unknown. Based on these observations, Cal_{EB} is likely one of the youngest vein generations present in the valley area (*Figure 3*).

Classification of breccia vein generations

According to BONS (2000), the term "breccia" when describing veins refers to veins containing clasts of varying sizes derived from the host rocks. In the studied valley, calcite veins containing a large proportion of clasts from the host lithology are classified as breccia veins. Clast size is a fundamental criterion for distinguishing breccia types, with various authors proposing different classification schemes. According to Spry (1969), breccias with clasts exceeding 5 mm are designated as tectonic breccias, while those with clasts between 5 mm and 1 mm are classified as fine-grained breccias, and those with clasts smaller than 1 mm are termed microbreccias. Higgins (1971) proposed a boundary of 0.2 mm between microbreccia and cataclasites. Laznicka (1988) distinguished mesobreccia from microbreccia based on a clast size threshold of 2 mm. The mineralogical composition of the cement and the crystallographic orientation have minimal influence on breccia classification (Woodcock & Mort 2008). Based on these criteria, two distinct breccia types have been identified within the valley: Cal_{BR1} and Cal_{BR2} (*Table I*). The Cal_{BR1} vein generation predominantly contains clasts smaller than 1 mm (*Figure 5*), categorizing them as microbreccia. In contrast, the Cal_{BR2} vein generation features clasts up to 4 mm in size (*Figure 7B, D*), classifying them as fine breccia. Both breccia types contain angular and rounded clasts, suggesting that brecciation involved not only mechanical fragmentation but also chemical processes (Jebrak 1997).

Within the Cal_{BR2} vein generation, clasts frequently form larger, spherical clusters (*Figure 2C*). These smaller clasts are typically fused and appear to be "floating" within the calcite cement, a characteristic feature of floating clast breccias (Chauvet 2019), as shown in *Figure 2C*. This mosaic arrangement of clasts suggests hydraulic brecciation driven by elevated fluid pressure**,** as described by Jebrak (1997). Floating clast breccias are typically associated with episodic hydraulic fracturing, leading to multiple cycles of brecciation and cementation (Chauvet 2019).

Fluid events

By analysing fluid inclusions trapped within calcite crystals, we aimed to determine the relative timing and physicochemical conditions of fluid migration events associated with mineral vein formation and structural evolution.

FIA-P and FIA-S fluid inclusions consist of fluorescent, liquid + vapour inclusions clearly visible under UV illumination (*Figure 10*), observed in the Cal_{B2} and Cal_{CR} vein generations. The blue, yellow, and red fluorescent inclusions contain hydrocarbons and occur as primary inclusions in the Cal_{B2} vein generation (*Figure 10A, B; Figure 3*) and as secondary inclusions in the Cal_{CR} vein generation (*Figure 10C, D; Figure 3*). The fluorescence colour of fluid inclusions is controlled by the relative proportions of aromatic and heteroatomic compounds within the hydrocarbon-bearing fluid and their ratio to normal alkanes (Bertrand et al. 1986, Oxtoby 2002, Skaare et al. 2011). The presence of three different fluorescence colours suggests the entrapment of hydrocarbon fluids with different compositions. The geochemical characteristics of migrating hydrocarbon-bearing fluids are largely influenced by the nature of their source rock and the thermal maturity of the hydrocarbons (McLimans 1987, Kihle 1995, Blanchet et al. 2003). According to Kihle (1995), immature oils usually fluoresce in the yellow-red spectrum under UV light, whereas fluorescence shifts towards the blue spectrum with increasing thermal maturity. Alteration processes such as water washing and biodegradation can modify the chemical composition of hydrocarbons, often resulting in a red shift in fluorescence (George et al. 2001). Skaare et al. (2011) also reported a correlation between the fluorescence colour of fluid inclusions and the °API gravity of the hydrocarbon phase. Based on this correlation, the fluorescence spectra of inclusions in the Cal_{B2} vein generations were analysed (*Figure 14*), providing insights into hydrocarbon inclusions with varying °API gravities.

In the Cal_{B2} vein generation, fluid inclusions displaying different UV fluorescence colours are closely associated along the same growth zones. The occurrence of fluid inclusions within a single FIA exhibiting different UV fluorescence colours has previously been documented in calcites from the TSZ quarry near Pécsvárad (Lukoczki et al. 2012). Given that hydrocarbon fluids typically exist as a homogeneous phase under subsurface conditions, the presence of petroleum inclusions with variable compositions within the same growth zone appears to contradict FIA theory (Chi et al. 2021). Selective adsorption of distinct hydrocarbon components during fluid inclusion entrapment can lead to minor compositional variations, resulting in fluorescence heterogeneity (Pironon & Bourdet 2008).

When fluid inclusions of different fluorescence colours occur within a single FIA, yet the coexistence of multiple hydrocarbon-bearing fluids of different compositions in the fracture system at the time of entrapment is unlikely, microscale segregation on the surface of the precipitating mineral is the most plausible explanation. This mechanism accounts for the spatial association of fluid inclusions with variable

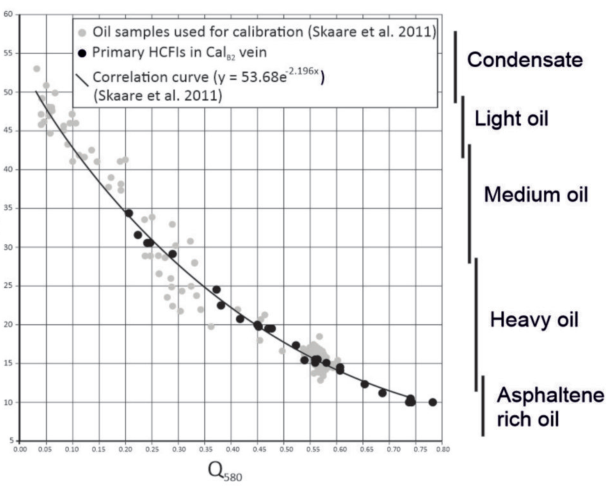

Figure 14. Correlation between the fluorescence colour of hydrocarbon-containing fluid inclusions and °API density (grey dots), as determined by Skaare et al. (2011). Black dots represent primary hydrocarbon-containing fluid inclusions with different fluorescence colour in the Cal_{B2} vein generation.

14. ábra. *Skaare et al. (2011) által meghatározott összefüggés a szénhidrogén-tartalmú fluidumzárványok fluoreszcens színe és °API sűrűsége között (szürke pontok). A fekete pontok a Cal_{B2} érgenerációban található eltérő fluoreszcens színnel rendelkező, elsődleges szénhidrogén-tartalmú fluidumzárványokat jelölik.*

fluorescence colours along the same planes or growth zones. The fluorescence spectra of the yellow and blue inclusions – interpreted as primary and secondary in origin, respectively (*Figure 12A*) – exhibit strong similarities to those documented in samples from Pécsvárad (LUKOCZKI et al. 2012). In addition to UV fluorescence spectroscopic analysis of calcite samples from Pécsvárad, microthermometric measurements were performed, revealing that the T_h(L+V→L) of hydrocarbon inclusions varied between 30 and 100 °C (LUKOCZKI et al. 2012). In the case of the Cal_{B2} vein generation analysed in this study, T_h(L+V→L) values of secondary inclusions ranged from 58 to 101 °C (*Figure 11*). At Árpádtető, located southwest of the Óbánya Valley and Pécsvárad quarry, LUKOCZKI & SCHUBERT (2014) described hydrocarbon-bearing fluid inclusions that appear yellowish-brown under normal light, but fluoresce blue under UV light. For these inclusions, the T_h(L+V→L) values ranged from 76 to 114 °C. The study did not clearly identify the potential source rock of the hydrocarbons.

In case of Pécsvárad, based on the organic matter type and thermal maturity of the host rock (Hosszúhetény Calcareous Marl Formation), it has been inferred that the hydrocarbon source rock responsible for fluid migration in the fracture systems was likely the marl itself. HAN et al. (2022) further supported this interpretation, based on biomarker analyses of hydrocarbon-bearing inclusions in marl and fracture-filling calcite from the Pécsvárad quarry.

To date, no organic geochemical investigations have been carried out on the marl and clayey limestone formations of the Komló Calcareous Marl Formation within the valley area. Consequently, there is no direct evidence that the hydrocarbons in the calcite veins were derived from these host rocks. The organic content of the Rékavölgy Siltstone (formerly Óbánya Aleurolite) Formation in the Réka Valley — running nearly parallel to the Óbánya Valley — was investigated by VARGA et al. (2007). Based on total organic carbon (TOC) content and the quantity of hydrocarbons released during pyrolysis, the black shale of the formation is considered an excellent petroleum source rock under suitable conditions, despite the strata currently exposed on the surface not having reached the oil generation window (R_o = 3.89–8.12% in laminated rock types, R_o = 2.14–3.29% in thin-bedded varieties). Additionally, a liptinite-rich interval of the Mecsek Coal Formation can also be considered a potential petroleum source rock, though its oil-generating potential is relatively low (TISSOT & WELTE 1984).

BADICS & VETŐ (2012) modelled the thermal maturity of these formations using borehole data from the northern foreland of the Mecsek and concluded that Early Jurassic formations there reached the oil window during the Cretaceous, implying the potential for oil generation at that time. However, while the source rock for the hydrocarbons trapped in these inclusions is likely among these three potential petroleum source rocks (Mecsek Coal Formation, Hosszúhetény Calcareous Marl Formation, and the Rékavölgy Siltstone Formation) the exact origin of the hydrocarbons in the calcite veins of the Óbánya Valley remains undetermined.

Among the samples from the Óbánya Valley area, the Cal_{B2} vein generation contains hydrocarbon-bearing fluid inclusions of primary (syntectonic) origin relative to vein formation. These inclusions are distributed along multiple parallel planes adjacent to the vein wall (*Figure 10A, B*), indicating that hydrocarbon migration was associated with this vein generation. However, orientation data suggest that the formation of the Cal_{B2} veins is linked to the folding, implying that the trapping of hydrocarbon inclusions occurred syntectonically relative to the folding event. The Cal_{CR} vein generation predates the Cal_{B2} vein generation, meaning that fluid inclusions identified as primary in the younger veins can be reinterpreted as secondary inclusions along minor fractures in the older vein generation based on their similar petrographic characteristics (*Figure 3*). Since there are no direct data available on the timing of vein formation, it can only be correlated with larger-scale tectonic events affecting the area. The presence of primary hydrocarbon-bearing fluid inclusions is associated with folding, which most likely developed during a Cretaceous deformation event. The organic-rich formations identified in the vicinity of the study area all predate this Cretaceous tectonic event. Therefore, any of these formations could potentially have acted as the source rock for the hydrocarbon-bearing fluids that migrated into the valley.

Non-fluorescent, liquid-phase fluid inclusions occur in the Cal_{B1-4}, Cal_{CR} (peripheral zone), Cal_{BR1}, and Cal_{BR2} vein generations (*Figure 9*). These inclusions range from 2 to 5 μm in size and are presumed to contain aqueous fluids. According to GOLDSTEIN & REYNOLDS (1994), such small, liquid-phase aqueous inclusions typically form below 50 °C. This suggests that these secondary fluid inclusions were likely trapped near the surface during a later-stage fluid migration event in the valley. The liquid-phase inclusions are typically arranged in planes that do not correspond to growth zones, indicating their secondary origin through fracture healing. Their small size, liquid-phase nature, and inferred low trapping temperature (below 50 °C) are indicative of a shallow fluid flow event.

Conclusions

In our study, we examined whether the fractures and veins observed along the Óbánya Valley, or specific groups of them, can be linked to expected fracture pattern related to folding, assuming that the large-scale fold geometry and orientation across the valley are similar to those identified at Bodzás Spring. In the Óbánya Valley, both a calcite-cemented fracture network and unmineralized cracks are present. Based on textural and microstructural characteristics, six vein generations have been identified, with their relative formation sequence established, except for Cal_{EB} (*Figure 3*). The veins and textural features suggest that Cal_{BR1} formed prekinematically relative to folding. In contrast, the orientation of the other vein generations aligns with fractures associated with a single deformation event (*Figure 3; Figure*

13A, B). The valley area underwent a sinistral displacement after folding, likely leading to the formation of the Cal_{BR2} vein generation (*Figure 3*).

Both aqueous and hydrocarbon-bearing fluid inclusions were trapped within the veins. Hydrocarbon-bearing inclusions of primary origin occur in Cal_{B2}, while secondary hydrocarbon inclusions are present in the Cal_{CR} veins. This observation is interpreted as evidence indicating that the hydrocarbon-bearing fluid inclusion in both vein generations was associated with the same fluid flow event. This suggests that the migration of hydrocarbon-bearing fluids occurred postkinematically relative to the folding event. Under UV illumination, these fluid inclusions exhibit blue, yellow, and red fluorescence, indicative of the presence of multiple oil types. Their close spatial association within the same FIA implies that a single hydrocarbon-bearing fluid migrated through the fracture system, with micro-scale fractionation occurring during fluid entrapment resulting in the various fluorescent colours.

To date, no Rock-Eval pyrolysis or TOC measurements have been published on the Komló Calcareous Marl Formation in the valley area. Previous studies have identified the Hosszúhetény Calcareous Marl Formation (LUKOCZKI et al. 2012, HAN et al. 2022) and the Rékavölgy Siltstone Formation (BADICS & VETŐ 2012) as excellent petroleum source rocks based on the maturity of their organic matter. Given that all potential source rocks are older than the deformation event possibly associated with hydrocarbon migration, unequivocally determining the origin of the parent fluid is currently not possible with the available data.

Acknowledgements

We thank Béla RAUCSIK and Sándor KÖRMÖS for their helpful advice on the topic of this manuscript. We also thank the National Research, Development and Innovation Office, National Scientific Research Funding Programme K-138919, for supporting the study. Finally, we thank Viktor GRANYÁK of the Department of Geology, University of Szeged, for preparing thin sections and providing helpful advice. We are grateful for the constructive and inspiring comments of Georgina LUKOCZKI, Gyula MAROS and László FODOR on the manuscript.

References – Irodalom

BADICS, B. & VETŐ, I. 2012: Source rocks and petroleum systems in the Hungarian part of the Pannonian Basin: The potential for shale gas and shale oil plays. – *Marine and Petroleum Geology* **31**, 53–69. https://doi.org/10.1016/j.marpetgeo.2011.08.015

BENKOVICS, L., MANSY, J.-L., CSONTOS, L. & BERGERAT, F. 1997: Folding in the Abaliget road cut (Mecsek Mts). – *Acta Geologica Hungarica* **40/4**, 425–440.

BERGERAT, F. & CSONTOS, L. 1988: Brittle tectonics and paleostressfields in the Mecsek and Villány Mountains (Hungary): correlations with the opening mechanisms of the Pannonian Basin. – *Acta Geologica Hungarica* **31/1–2**, 81–100.

BERKOWITZ, B. 2002: Characterizing flow and transport in fractured geological media: A review. – *Advances in Water Resources* **25**, 861–884. https://doi.org/10.1016/S0309-1708(02)00042-8

BERTRAND, P., PITTON, J.-L. & BERNAUD, C. 1986: Fluorescence of sedimentary organic matter in relation to its chemical composition. – *Organic Geochemistry* **10**, 641–647. https://doi.org/10.1016/0146-6380(86)90061-6

BILIK, I. 1980: Lower Cretaceous submarine (rift) volcanism in South Transdanubia (South Hungary). – In: BISZTRICSÁNY, E. & SZEIDOVITZ, GY. (eds): *Proceedings of the 17th Assembly of the European Seismological Congress*, 563–576, Akadémiai Kiadó, Budapest. https://doi.org/10.1016/b978-0-444-99662-6.50042-3

BLANCHET, A., PAGEL, M., WALGENWITZ, F. & LOPEZ, A. 2003: Microspectrofluorimetric and microthermometric evidence for variability in hydrocarbon fluid inclusions in quartz overgrowths: implications for inclusion trapping in the Alwyn North field, North Sea. – *Organic Geochemistry* **34**, 1477–1490. https://doi.org/10.1016/j.orggeochem.2003.08.003

BONS, P. D. 2000: The formation of veins and their microstructures. – In: JESSELL, M. W. & URAI, J. L. (eds): *Stress, Strain and Structure: a volume in honour of Win D. Means*. Volume 2, Journal of the Virtual Explorer https://doi.org/10.3809/jvirtex.2000.0007

BONS, P. D., ELBURG, M. A. & GOMEZ-RIVAS, E. 2012: A review of the formation of tectonic veins and their microstructures. – *Journal of Structural Geology* **43**, 33–62. https://doi.org/10.1016/j.jsg.2012.07.005

BÖCKH J. 1880: *Adatok a Mecsekhegység és dombvidéke jurakorabeli lerakódások ismeretéhez – I. Stratigraphiai rész.* – Magyar Tudományos Akadémia könyvkiadóhivatal, 24–36.

BURKHARD, M. 1993: Calcite twins, their geometry, appearance and significance as stress-strain markers and indicators of tectonical regime: a review. – *Journal of Structural Geology* **15**, 351–368. https://doi.org/10.1016/0191-8141(93)90132-t

CHAUVET, A. 2019: Structural control of ore deposits: The role of pre-existing structures ont he formation of mineralised vein systems. – *Minerals* **9**, 56 https://doi.org/10.3390/min9010056

CHI, G., DIAMOND, L. W., LU, H., LAI, J. & CHU, H. 2021: Common problems and pitfalls in fluid inclusion study: A review and discussion. – *Minerals* **11/1**, 7 https://doi.org/10.3390/min11010007

CSÁSZÁR G. & HAAS J. (eds) 1983: *Magyarország litosztatigráfiai formációi*. – MÁFI, Budapest.

CSONTOS, L., BENKOVICS, L., BERGERAT, F., MANSY, J.-L. & WÓRUM, G. 2002: Tertiary deformation history from seismic section study and fault analysis in a former European Tethyan margin (the Mecsek–Villány area, SW Hungary). – *Tectonophysics* **357**, 81–102. https://doi.org/10.1016/S0040-1951(02)00363-3

DAVIS, G. H., REYNOLDS, S. J. & KLUTH, C. F. 2011: *Structural Geology of Rocks and Regions.* – John Wiley and Sons, New York, 148 p.

DICKSON, J. A. D. 1965: A Modified Staining Technique for Carbonates in Thin Section. – *Nature* **205**, 587 (1965). https://doi.org/10.1038/205587a0

DIAMOND, L. W. 2003: Glossary: Terms and symbols used in fluid inclusion studies. – In: SAMSON, I., ANDERSON, A. & MARSHALL, D. (eds): *Fluid Inclusions: Analysis and Interpretation* – Mineralogical Association of Canada Short Course Series, **32**.

FERILL, D. A., MORRIS, A. P., EVANS, M. A., BURKHARD, M., GROSHONG, R. H. & ONASCH, C. M. 2004: Calcite twin morphology: a low-temperature deformation geothermometer. – *Journal of Structural Geology* **25**, 1521–1529. https://doi.org/10.1016/j.jsg.2003.11.028

FISCHER, M. P., HIGUERA-DÍAZ, I. C., EVANS, M. A., PERRY, E. C. & LEFTICARIU, L. 2009: Fracture-controlled paleohydrology in a map-scale detachment fold: Insights from the analysis of fluid inclusions in calcite and quartz veins. – *Journal of Structural Geology* **31**, 1490–1510. https://doi.org/10.1016/j.jsg.2009.09.004

FODOR, L., CSONTOS, L., BADA, G., GYÖRFI, I. & BENKOVICS, L. 1999: Tertiary tectonic evolution of the Pannonian Basin System and neighbouring orogens: a new synthesis of palaeostress data. – In: DURAND, B., JOLIVET, L., HORVÁTH, F. & SÉRANNE, M. (eds): The Mediterranean Basins: Tertiary Extension within the Alpine Orogen. *Geological Society, London, Special Publications* **156**, 295–334. https://doi.org/10.1144/gsl.sp.1999.156.01.15

FOSSEN H. 2016: *Structural Geology.* – Cambridge University Press, Cambridge, 123 p. https://doi.org/10.1017/9781107415096

GALÁCZ A., HABLY L. & SZENTE I. 1992: *Kirándulásvezető a Magyarhoni Földtani Társulat Őslénytani-Rétegtani Szakosztályának 1992. június 19–20-i mecseki terepbejárásához.* – Magyarhoni Földtani Társulat, Budapest, 17 p.

GEORGE, S. C., RUBLE, T. E., DUTKIEWICZ, A. & EADINGTON, P. E. 2001: Assessing the maturity of oil trapped in fluid inclusions using molecular geochemistry data and visually-determined fluorescence colours. – *Applied Geochemistry* **16**, 451–473. https://doi.org/10.1016/s0883-2927(00)00051-2

GÉCZY, B. 1973: Plate tectonics and paleogeography in the East-Mediterranean Mesozoic. – *Acta Geologica Hungarica* **17**, 421–428.

GOLDSTEIN, R. H. & REYNOLDS T. J. 1994: Systematics of Fluid Inclusions in Diagenetic Minerals. – *SEPM Society for Sedimentary Geology* **31**. https://doi.org/10.2110/scn.94.31

HAAS J. 1994: *Magyarország földtana, mezozóikum* – Egyetemi jegyzet, ELTE Kiadó, 119 p.

HAAS, J., HÁMOR, G., JÁMBOR, Á., KOVÁCS, S., NAGYMAROSY, A. & SZEDERKÉNYI, T. 2012: *Geology of Hungary*. – Springer, 244 p. https://doi.org/10.1007/978-3-642-21910-8_2

HAN, Y., NOAH, M., LÜDERS, V., KÖRMÖS, S., SCHUBERT, F., POETZ, S., HORSFIELD, B. & MANGELSDORF, K. 2022: Fractionation of hydrocarbons and NSO-compounds during primary oil migration revealed by high resolution mass spectrometry: Insights from oil trapped in fluid inclusions. – *International Journal of Coal Geology* **254**, 103974. https://doi.org/10.1016/j.coal.2022.103974

HARANGI SZ. & ÁRVÁNÉ-SÓS E. 1993: A Mecsek hegység alsókréta vulkáni kőzetei I. Ásvány és kőzettan (Early Cretaceous volcanic rocks of the Mecsek mountains, South Hungary I. Mineralogy and petrology). – *Földtani Közlöny* **123/2**, 129–165.

HETÉNYI R. 1966: A mecseki középsőliász tagolása. – *A Magyar Állami Földtani Intézet Évi Jelentése az 1964. évről*, 23–27.

HIGGINS, M. W. 1971: Cataclastic Rocks. – *Professional Paper, United States Geological Survey* **687**, 97 p. https://doi.org/10.3133/pp687

HRABOVSZKI E., KÖRMÖS S., TÓTH E., STEINBACH G., M. TÓTH T. & SCHUBERT F. 2023: Ásványos erek a Kantavári kőfejtőben. – In: RAUCSIKNÉ VARGA A. (szerk.): *13. Kőzettani és Geokémiai Vándorgyűlés: Előadás- és poszterkivonatok.* Szegedi Tudományegyetem TTIK, Ásványtani, Geokémiai és Kőzettani Tanszék, 13–14.

JEBRAK, M. 1997: Hydrothermal breccias in vein-type ore deposits; A review of mechanisms, morphology and size distribution. – *Ore Geology Reviews* **12**, 111–134. https://doi.org/10.1016/s0169-1368(97)00009-7

KIHLE, J. 1995: Adaptation of fluorescence excitation-emission micro-spectroscopy for characterisation of single hydrocarbon fluid inclusions. – *Organic Geochemistry* **23**, 1029–1042. https://doi.org/10.1016/0146- 6380(95)00091-7

KONRÁD GY., SEBE K., HALÁSZ A. & HALMAI Á. 2010: A Délkelet-Dunántúl földtani fejlődéstörténete – recens analógiák. – *Földrajzi Közlemények* **134/3**, 251–265.

KUBOVICS, I., SZABÓ, CS., HARANGI, SZ. & JÓZSA, S. 1990: Petrology and petrochemistry of Mesozoic magmatic suites in Hungary and adjacent areas – an overview. – *Acta Geodaetica, Geophysica et Montanistica*, **25/3–4**, 345– 371.

LADÁNYI L. 2021: *Szerkezetföldtani és petrográfiai megfigyelések az Óbányai-völgyben (Kelet-Mecsek).* – szakdolgozat, Szegedi Tudományegyetem, 49 p.

LADÁNYI L., HRABOVSZKI E. & SCHUBERT F. 2023: Töréses és képlékeny szerkezeti elemekhez kapcsolódó érrendszerek az óbányai Öreg-patak völgyben (Keleti-Mecsek). – In: RAUCSIKNÉ VARGA A. (szerk.): *13. Kőzettani és Geokémiai Vándorgyűlés: Előadás és poszter kivonatok* Szegedi Tudományegyetem TTIK, Ásványtani, Geokémiai és Kőzettani Tanszék, 37.

LAZNICKA, P. 1988: Breccias and Coarse Fragmentites. Petrology, Environments, Associations, Ores. – *Developments in Economic Geology Series* **25**. Amsterdam, Elsevier, 832 p.

LINDHOLM, R. C. & FINKELMAN, R. B. 1972: Calcite staining: Semiquantitative determination of ferrous iron. – *Journal of Sedimentary Research* **42/1**, 239–242. https://doi.org/10.1306/74d724fa-2b21-11d7- 8648000102c1865d

LUKOCZKI, G. & SCHUBERT, F. 2014: Traces of hydrocarbon migration in the Central Mecsek Mountains. – *Földtani Közlöny* **144/4**, 403–407.

LUKOCZKI G., SCHUBERT F. & HÁMORNÉ V. M. 2012: Szénhidrogén-migráció nyomai Pécsvárad környékén (Mecsek hegység). – *Földtani Közlöny* **142/3**, 229–242.

LUNINA, O. 2019: An overview of clastic dikes: significance for earthquake study. – *Geodynamics & Tectonophysics* **10/2**, 483–506. http://dx.doi.org/10.5800/GT-2019-10-2-0423

McLimans, R. K. 1987: The application of fluid inclusions to migration of oil and diagenesis in petroleum reservoirs. – *Applied Geochemistry* **2**, 585–603. https://doi.org/10.1016/0883-2927(87)90011-4

Moretti, I. 1998: The role of faults in hydrocarbon migration. – *Petroleum Geosience* **4/1**, 81–94. https://doi.org/10.1144/petgeo.4.1.81

Munz, I. A. 2001: Petroleum inclusions in sedimentary basins: systematics, analytical methods and applications. – *Lithos* **55**, 195–212. https://doi.org/10.1016/s0024-4937(00)00045-1

Nagy E. 1969: A Mecsek hegység alsóliász kőszénösszlete. – *Földtan – Ősföldrajz – MÁFI Évkönyv* **51/2**, 289–318.

Nelson, D. R. 2001: An assessment of the determination of depositional ages for precambrian clastic sedimentary rocks by U-Pb dating of detrital zircons. – *Sedimentary Geology* **141–142**, 37–60. https://doi.org/10.1016/s0037-0738(01)00067-7

Némedi Varga Z. 1983: A Mecsek hegység szerkezetalakulása az alpi hegységképződési ciklusban. – *A Magyar Állami Földtani Intézet Évi Jelentése az 1981 évről*, 467–484.

Némedi Varga Z. 1998: A Mecsek és a Villányi egység jura képződményeinek rétegtana. – In: Bérczi I. & Jámbor Á. (szerk.): *Magyarország geológiai képződményeinek rétegtana*. MOL Rt. – MÁFI, Budapest, 319–336.

Odling, N. E. 1997: Scaling and connectivity of joint systems in sandstones from western Norway. – *Journal of Structural Geology* **19/10**, 1257–1271. https://doi.org/10.1016/s0191-8141(97)00041-2

Oxtoby, N. H. 2002: Comments on: Assessing the maturity of oil trapped in fluid inclusions using molecular geochemistry data and visually-determined fluorescence colours. – *Applied Geochemistry* **17/10**, 1371–1374. https://doi.org/10.1016/s0883-2927(02)00026-4

Petrik A. 2009: A villányi-hegységi mezozoos képződmények mikrotektonikai méréseinek értelmezése. – *Földtani Közlöny* **139/3**, 217–236.

Pironon, J. & Bourdet, J. 2008: Petroleum and aqueous inclusions from deeply buried reservoirs. Experimental simulations and consequences for overpressure estimates. – *Geochimica et Cosmochimica Acta* **72**, 4916–4928. https://doi.org/10.1016/j.gca.2008.07.019

Püspöki, Z., Forgács, Z., Kovács, Zs., Kovács, E., Soós-Kablár, J., Jäger, L., Pusztafali, J., Kovács, Z., Demeter, G., McIntosh, R. W., Buday, T., Kozák, M. & Verbőci, J. 2012: Stratigraphy and deformation history of the Jurassic coal bearing series in the Eastern Mecsek (Hungary). – *International Journal of Coal Geology* **102**, 35–51. https://doi.org/10.1016/j.coal.2012.07.009

Ramsay, J. G. 1967: *Folding and Fracturing fo Rocks*. – McGraw-Hill, New York, 568 p. https://doi.org/10.1126/science.160.3826.410

Raucsik B. 2012: Komlói Mészmárga Formáció. – In: Főzy I. (szerk.): *Magyarország litosztatigráfiai alapegységei – Jura.* Magyarhoni Földtani Társulat, Budapest, 174–176.

Sebe, K. 2021: Structural features in the Miocene sediments of the Pécs-Danitzpuszta sand pit (SW Hungary). – *Földtani Közlöny* **151/4**, 411–422. https://doi.org/10.23928/foldt.kozl.2021.151.4.411

Sebe, K. & Pazonyi, P. 2025: Late Neogen-Quaternary exhumation of the Tisza unit basement carbonates based on paleontological data: Villány Hills, SW Pannonian Basin. – *Földtani Közlöny* **155/1**, 21–35. https://doi.org/10.23928/foldt.kozl.2025.155.1.21

Seilacher, A. 1969: Fault-graded beds interpreted as seismites. – *Sedimentology* **13**, 155–159. https://doi.org/10.1111/j.1365-3091.1969.tb01125.x

Skaare, B. B., Kihle, J. & Torsvik, T. 2011: Biodegradation of crude oil as potential source of organic acids in produced water. – In: Lee, K. & Neff, J. (eds): *Produced Water: Environmental Risks and Advances in Mitigation Technologies.* Springer, New York, 115–126. https://doi.org/10.1007/978-1-4614-0046-2_4

Spry, A. 1969: *Metamorphic Textures*. – Pergamon Press, Oxford, 350 p. https://doi.org/10.1180/minmag.1970.037.291.19

Sztanó O. & Magyar I. 2023: Neogén – Felső miocén – pliocén. – In: Babinszki E., Piros O., Csillag G., Fodor L., Gyalog L., Kercsmár ZS., Less Gy., Lukács R., Sebe K., Selmeczi I., Szepesi J. & Sztanó O. (szerk.): *Magyarország litosztatigráfiai egységeinek leírása II. – Kainozoos képződmények*. Szabályozott Tevékenységek Felügyeleti Hatósága, Budapest, 117–119.

Tissot, B. & Welte, D. H. 1984: *Petroleum formation and occurrence*. – Springer-Verlag, New York, 699 p. https://doi.org/10.1007/978-3-642-87813-8

Twiss, R. J. & Moores, E. M. 1992: *Structural Geology*. – Freeman and Company, New York, 532 p. https://doi.org/10.1002/gj.3350290408

Van der Pluijm, B. & Marshak, S. 2004: *Earth Structure: An Introduction to Structural Geology and Tectonics*. – Norton & Compan, New York, 656 p.

Varga A., Raucsik B., Hámorné V. M. & Rostási Á. 2007: Az Óbányai Aleurolit Formáció fekete palájának izotóp-geokémiai és szénhidrogén-genetikai jellemzése. – *Földtani Közlöny* **137/4**, 449–472.

Velledits, F., Híves, T. & Bársony, E. 1986: A Jurassic–lower Cretaceous profile in Óbánya valley (Mecsek Mts., Hungary). – *Annales Universitatis Scientiarium Budapestinensis, Section Geologica* **26**, 159–175.

Vörös, A. 1993: Redefinition of the Reitzi Zone at its type region (Balaton area, Hungary) as the basal zone of the Ladinian. – *Acta Geologica Hungarica* **36/1**, 15–31.

Wein Gy. 1967: Délkelet-Dunántúl hegységszerkezeti egységeinek összefüggései az óalpi ciklusban. – *Földtani Közlöny* **97/3**, 286–293.

Woodcock, N. H. & Mort, K. 2008: Classification of fault breccias and related fault rocks. – *Geological Magazine* **145/3**, 435–440. https://doi.org/10.1017/s0016756808004883

Manuscript received: 23.03.2025.

Appendix 1 – 1. melléklet

Appendix 1. Orientation data measured at the Bodzás Spring and sampling points, as well as notes on the outcrops.
1. melléklet. *A Bodzás-forrásnál és a mintavételi pontoknál mért orientációs adatok, valamint a feltárásokra vonatkozó jegyzetek.*

Sampling point	Dip direction	Dip angel	Note	Stream side
Bodzás Spring	263°	37°	Bedding plane, small fold	left
Bodzás Spring	266°	41°	Bedding plane, small fold	left
Bodzás Spring	262°	44°	Bedding plane, small fold	left
Bodzás Spring	260°	41°	Bedding plane, small fold	left
Bodzás Spring	266°	39°	Bedding plane, small fold	left
Bodzás Spring	275°	46°	Bedding plane, small fold	left
Bodzás Spring	276°	56°	Bedding plane, small fold	left
Bodzás Spring	270°	46°	Bedding plane, small fold	left
Bodzás Spring	272°	47°	Bedding plane, small fold	left
Bodzás Spring	269°	53°	Bedding plane, small fold	left
Bodzás Spring	272°	44°	Bedding plane, small fold	left
Bodzás Spring	278°	61°	Bedding plane, small fold	left
Bodzás Spring	265°	34°	Bedding plane, small fold	left
Bodzás Spring	280°	45°	Bedding plane, small fold	left
Bodzás Spring	144°	37°	Bedding plane, small fold	right
Bodzás Spring	153°	27°	Bedding plane, small fold	right
Bodzás Spring	158°	27°	Bedding plane, small fold	right
Bodzás Spring	146°	26°	Bedding plane, small fold	right
Bodzás Spring	143°	35°	Bedding plane, small fold	right
Bodzás Spring	211°	18°	Bedding plane, small fold	right
Bodzás Spring	231°	11°	Bedding plane, small fold	right
Bodzás Spring	133°	27°	Bedding plane, small fold	right
Bodzás Spring	145°	34°	Bedding plane, small fold	right
Bodzás Spring	154°	23°	Bedding plane, small fold	right
Bodzás Spring	149°	21°	Bedding plane, small fold	right
Bodzás Spring	155°	34°	Bedding plane, small fold	right
OB20/01	347°	88°	Calcite vein, Sample 1	right
OB20/01	67°	80°	Fracture	right
OB20/01	64°	80°	Fracture plane	right
OB20/01	116°	86°	Calcite	right
OB20/01	3°	87°	Calcite vein, 1 cm	right
OB20/01	116°	84°	Calcite plane	right
OB20/01	8°	89°	Calcite vein	right
OB20/01	329°	84°	Calcite	right
OB20/01	281°	84°	Calcite	right
OB20/01	110°	88°	Calcite vein	right
OB20/01	114°	85°	Calcite	right
OB20/02	280°	88°	Fracture	left
OB20/02	266°	88°	Fracture plane	left
OB20/02	249°	6°	Layer	left
OB20/02	247°	11°	Layer	left
OB20/02	158°	88°	Fracture plane	left

Appendix 1 – 1. melléklet

Appendix 1. continued
1. melléklet folytatása

Sampling point	Dip direction	Dip angel	Note	Stream side
OB20/02	156°	87°	Fracture	left
OB20/02	156°	87°	Fracture	left
OB20/02	337°	89°	Calcite 1 cm	left
OB20/02	334°	80°	Fracture	left
OB20/02	344°	85°	Calcite vein, Sample 2	left
OB20/02	212°	16°	Layer	right
OB20/03	333°	84°	Fracture, Sample 3	right
OB20/03	273°	85°	Fracture plane	right
OB20/03	225°	33°	Fracture plane	right
OB20/03	291°	87°	Fracture plane	right
OB20/04	297°	86°	Thin calcite vein 15 cm	left
OB20/04	116°	87°	Sample 4, thin calcite vein	left
OB20/04	192°	14°	Layer	left
OB20/04	174°	15°	Layer	left
OB20/04	293°	88°	Fracture	left
OB20/04	237°	89°	Fracture plane	left
OB20/04	84°	80°	Fracture	left
OB20/04	90°	77°	Fracture plane	left
OB20/04	275°	86°	Thin calcite vein	left
OB20/04	291°	82°	Thin vein	left
OB20/04	288°	89°	Thin vein, 4. Sample	left
OB20/04	269°	90°	Calcite vein, many zones + Sample 4	left
OB20/05	106°	89°	Sample 5, Thin vein	left
OB20/05	291°	79°	Thin vein	right
OB20/05	288°	76°	Thin calcite vein	right
OB20/05	20°	66°	Fracture	right
OB20/05	21°	64°	Fracture plane	right
OB20/05	275°	81°	Fracture plane	right
OB20/06	23°	85°	Sample 6, zoned folded vein, Cal_{CR} vein generation	left
OB20/07	205°	10°	Shear plane, highly unstable	right
OB20/07	136°	11°	Sample 7, reverse fault, calcite, Cal_{BR1}	right
OB20/08	168°	75°	Calcite vein	left
OB20/08	166°	86°	Calcite vein	left
OB20/08	182°	72°	Calcite vein	left

Appendix 2 – 2. melléklet

Appendix 2. Orientation data of bedding planes from the Óbánya Valley.
2. melléklet. *Réteglapok orientációs adatai az Óbányai-völgyből.*

Measurement point	Dip direction	Dip angel
1/1	235°	28°
1/3	316°	16°
1/4	313°	15°
1/5	223°	29°
1/5	237°	21°
1/5	237°	19°
1/6	222°	38°
1/6	222°	28°
1/7	263°	37°
1/7	266°	41°
1/7	262°	44°
1/7	260°	41°
1/7	266°	39°
1/7	275°	46°
1/7	276°	56°
1/7	270°	46°
1/7	272°	47°
1/7	269°	53°
1/7	272°	44°
1/7	278°	61°
1/7	265°	34°
1/7	280°	45°
1/7	144°	37°
1/7	153°	27°
1/7	158°	27°
1/7	146°	26°
1/7	143°	35°

Measurement point	Dip direction	Dip angel
1/7	211°	18°
1/7	231°	11°
1/7	133°	27°
1/7	145°	34°
1/7	154°	23°
1/7	149°	21°
1/7	155°	34°
1/8	177°	25°
1/8	172°	27°
1/8	177°	25°
1/8	179°	28°
1/9	204°	18°
1/9	210°	19°
1/10	207°	23°
1/10	222°	11°
1/11	203°	09°
1/13	221°	25°
1/13	243°	18°
1/13	213°	16°
1/15	266°	12°
1/15	266°	14°
1/15	282°	24°
1/15	264°	17°
2/1	313°	10°
2/1	324°	11°
2/2	305°	27°
2/2	290°	22°

Appendix 2 – 2. melléklet

Appendix 2. continued
2. melléklet folytatása

Measurement point	Dip direction	Dip angel
2/2	310°	29°
2/2	296°	26°
2/3	294°	08°
2/3	304°	14°
2/3	292°	10°
2/6	280°	05°
2/6	285°	05°
2/6	237°	05°
2/7	193°	11°
2/7	263°	08°
2/9	298°	06°
2/9	252°	14°
2/11	317°	04°
2/11	331°	03°
2/12	280°	05°
2/12	298°	04°
2/13	19°	67°
2/14	232°	07°
2/14	263°	08°
2/15	201°	10°
2/15	157°	16°
2/15	168°	09°
2/16	249°	06°
2/16	247°	11°
2/16	212°	16°
2/17	248°	09°
2/17	213°	09°

Measurement point	Dip direction	Dip angel
2/18	266°	05°
2/18	218°	07°
2/20	161°	15°
2/20	166°	18°
2/21	194°	19°
2/21	148°	15°
2/22	192°	14°
2/22	174°	15°
2/25	209°	22°
2/25	197°	19°
2/25	205°	19°
2/25	179°	16°
2/25	205°	15°
2/26	29°	25°
2/26	28°	24°
2/28	232°	19°
2/28	190°	28°
2/28	100°	13°
2/29	15°	09°
2/29	39°	09°